Phytopathology® • 2023 • 113:960-974 • https://doi.org/10.1094/PHYTO-06-22-0234-R

Bacteriology

Two *Xylella fastidiosa* subsp. *multiplex* Strains Isolated from Almond in Spain Differ in Plasmid Content and Virulence Traits

M. Román-Écija,[1] J. A. Navas-Cortés,[1] M. P. Velasco-Amo,[1] L. F. Arias-Giraldo,[1] L. M. Gómez,[2] L. De La Fuente,[2,†] and B. B. Landa[1,†]

[1] Department of Crop Protection, Institute for Sustainable Agriculture, Consejo Superior de Investigaciones Científicas, Córdoba, Spain
[2] Department of Entomology and Plant Pathology, Auburn University, Auburn, AL, U.S.A.
Accepted for publication 13 December 2022.

Abstract

The plant-pathogenic bacterium *Xylella fastidiosa* is a major threat to agriculture and the environment worldwide. Recent devastating outbreaks in Europe highlight the potential of this pathogen to cause emergent diseases. *X. fastidiosa* subsp. *multiplex* ESVL and IVIA5901 strains that belong to sequence type 6 were isolated from almond orchards within the outbreak area in Alicante province (Spain). Both strains share more than 99% of the chromosomal sequences (average nucleotide identity), but the ESVL strain harbors two plasmids (pXF64-Hb_ESVL and pUCLA-ESVL). Here, virulence phenotypes and genome content were compared between both strains, using three strains from the United States as a reference for the phenotypic analyses. Experiments in microfluidic chambers, used as a simulation of xylem vessels, showed that twitching motility was absent in the IVIA5901 strain, whereas the ESVL strain had reduced twitching motility. In general, both Spanish strains had less biofilm formation, less cell aggregation, and lower virulence in tobacco compared with U.S. reference strains. Genome analysis of the two plasmids from ESVL revealed 51 unique coding sequences that were absent in the chromosome of IVIA5901. Comparison of the chromosomes of both strains showed some unique coding sequences and single-nucleotide polymorphisms in each strain, with potential deleterious mutations. Genomic differences found in genes previously associated with adhesion and motility might explain the differences in the phenotypic traits studied. Although additional studies are necessary to infer the potential role of *X. fastidiosa* plasmids, our results indicate that the presence of plasmids should be considered in the study of the mechanisms of pathogenicity and adaptation in *X. fastidiosa* to new environments.

Keywords: almond leaf scorch, biofilm, *Prunus dulcis*, quarantine, virulence, xylem

Xylella fastidiosa is a gram-negative, xylem-limited bacterium native to the Americas that is transmitted exclusively in nature by xylem fluid-feeding insects (Almeida et al. 2019; Sicard et al. 2018). Currently, the *X. fastidiosa* host range exceeds 600 plant species (Delbianco et al. 2022). The bacterium causes a variety of diseases in crops of high economic importance, including grapevine (Pierce's disease), citrus (citrus variegated chlorosis), almond (almond leaf scorch), olive (olive quick decline syndrome), and oaks (oak leaf scorch), with a huge economic impact on agriculture, public gardens, and the environment (Saponari et al. 2017). *X. fastidiosa* is a genetically diverse species made up of basically three subspecies and multiple genetic lineages grouped as sequence types (STs) (Denancé et al. 2019; Marcelletti and Scortichini 2016). Although each ST may have a different host range, there is some overlap, with some STs infecting several important host crops (Delbianco et al. 2022; Nunney et al. 2019; Sicard et al. 2018).

In Europe, where *X. fastidiosa* has been categorized as a quarantine pathogen since 1989, the bacterium was not detected in nature until 2013, when an outbreak of *X. fastidiosa* on olive trees was reported in the Salento region of Italy (Saponari et al. 2017). The unprecedented massive mortality of olive trees in that area heightened concerns on the risk of *X. fastidiosa* spreading across Europe. As a result, mandatory surveys of EU member states were conducted, revealing that the bacterium was also established in agricultural fields and natural environments in the Balearic Islands and Alicante, Spain (Moralejo et al. 2020); Tuscany, Italy (Saponari et al. 2019); Corsica and the Provence-Alpes-Côte d'Azur region, France (EFSA PLH et al. 2019); and Vila Nova de Gaia, Portugal (EFSA PLH et al. 2019).

The adaptability of this bacterium to colonize new hosts and environments has been associated with its ability to acquire new genetic information (Potnis et al. 2019), which has been proposed as one of the causes of the emergence of new diseases caused by this plant pathogen (Vanhove et al. 2019). The presence of mobile genetic elements in *X. fastidiosa* strains that are an important source of diversity, such as plasmids, prophages, insertion sequence elements, and transposons, suggests active horizontal gene transfer (Monteiro-Vitorello et al. 2005), which, together with its natural competence ability, plays an important role in the genetic diversity of *X. fastidiosa* strains (Kandel et al. 2017).

Plasmids have a dominant role in the horizontal transfer of genetic information among bacteria, allowing DNA transfer between genera, phyla, and even major domains (Sørensen et al. 2005). Several studies have shown that some plasmids may confer adaptative

†Corresponding authors: L. De La Fuente; lzd0005@auburn.edu, and B. B. Landa; blanca.landa@csic.es

Funding: Support was provided by the AEI-INIA Spain and the Spanish Olive Oil Interprofessional (grant E-RTA2017-00004-C06-02), European Union's Horizon 2020 Framework Research Programme XF-ACTORS (*Xylella fastidiosa* Active Containment Through a Multidisciplinary-Oriented Research Strategy; grant 727987), European Cooperation in Science and Technology (COST) Action CA16107 Euro-Xanth Short Term Scientific Missions fellowship (M. Román-Écija), Thematic Interdisciplinary Platform on *X. fastidiosa* from Consejo Superior de Investigaciones Científicas (PTI-SolXyl), Alabama Agricultural Experiment Station Hatch Program (L. De La Fuente). L. De La Fuente was a recipient of a research fellowship awarded by the Organization for Economic Cooperation and Development, Cooperative Research Programme, during the writing of this manuscript. M. P. Velasco-Amo was a recipient of a contract financed by the Consejo Superior de Investigaciones Científicas Intramural Project 201840E111.

e-Xtra: Supplementary material is available online.

The author(s) declare no conflict of interest.

traits, the acquisition of virulence genes, or the capacity to take new genes from the environment through the conjugative type IV secretion system (Burbank and Van Horn 2017; Sengupta and Austin 2011; Sørensen et al. 2005; Vivian et al. 2001). Several studies have revealed the presence of native plasmids in strains of *X. fastidiosa* isolated from different plant species, including almond, grape, oak, peach, plum, oleander, and mulberry (Chen et al. 2005; Colnaghi Simionato et al. 2007; Guilhabert et al. 2006; Hendson et al. 2001; Pooler et al. 1997; Simpson et al. 2000; Stenger et al. 2010), and their sequences have been compared to assess variability (Pierry et al. 2020). However, little is known concerning the influence of those plasmids in specific phenotypic traits related to the colonization and pathogenicity of *X. fastidiosa* plasmid-harboring strains.

In *X. fastidiosa*-induced diseases, symptoms are associated with the ability of the bacterium to form aggregates that occlude xylem vessels producing water and nutrient stresses (Hopkins 1989). It is known that bacterial aggregation and biofilm development are crucial for the establishment of pathogenic bacteria in host plants (Bogino et al. 2013). Biofilm formation, cell aggregation, and attachment of cells in the xylem vessels are mediated by type I and IV pili in *X. fastidiosa* (De La Fuente et al. 2007b, 2008; Li et al. 2007). The presence of type IV pili, which is responsible for twitching motility, might also contribute to *X. fastidiosa* spread through xylem vessels and colonization of different parts of the host plant (Meng et al. 2005). Although both types of pili are important in the *X. fastidiosa* life cycle, the process of pathogenesis is complex, and other factors could also be involved (Bogino et al. 2013; Koide et al. 2004). Some structures present on the cell surface, such as nonfimbrial and hemagglutinin adhesins, play a key role during surface attachment, biofilm formation, and cell aggregation, as well as in the virulence of *X. fastidiosa* (Bogino et al. 2013; Feil et al. 2007; Guilhabert and Kirkpatrick 2005; Li et al. 2007). Several studies identified other molecular components playing a role in disease development. These include the major outer membrane protein (Chen et al. 2017), regulatory proteins involved in the detection of oxidative stress (Wang et al. 2017), cell-cell signaling mediated by a fatty acid diffusible signaling factor (Newman et al. 2004), the response regulator *GacA* of some pathogenicity genes involved in sensing environmental signals (Shi et al. 2007), and the putative acyl-coenzyme A synthase (Hao et al. 2017).

In this study, we characterized the phenotypic traits potentially associated with infection and disease development of two strains of *X. fastidiosa* subsp. *multiplex* belonging to ST6, named ESVL and IVIA5901. Both strains were isolated in 2017 from almond trees showing almond leaf scorch symptoms from orchards located in the Spanish outbreak occurring at the Guadalest Valley in Alicante province (Valencian Community). In this area, only *X. fastidiosa* subsp. *multiplex* ST6 has been identified so far (Marco-Noales et al. 2021). Currently, the *X. fastidiosa* demarcated area in this region covers an extension of more than 136,200 hectares. This outbreak represents one of the largest eradication campaigns ever carried out in Europe, with around 12,500 orchards and over 1,100 hectares and 90,000 trees already destroyed as of November 2021 (DOGV 2021). Initial genome analysis of both Spanish *X. fastidiosa* strains indicated that the strains share more than 99% of the chromosomal sequences (average nucleotide identity), but the most notorious difference between these strains was the presence of two plasmids detected only in the ESVL strain (Giampetruzzi et al. 2019). We evaluated in vitro fundamental traits related to colonization and virulence of *X. fastidiosa*, including biofilm formation, cell aggregation, and cell motility, as well as virulence in the model plant tobacco, using as comparison three reference strains from the United States. Finally, we performed comparative genomic analyses of the complete circularized sequences of the two Spanish strains to identify differences in plasmid or chromosomal content that could be correlated with the observed phenotypic differences.

Materials and Methods

Bacterial strains and culture conditions

Two *X. fastidiosa* subsp. *multiplex* strains were used in the study, isolated from almond trees (IVIA5901 and ESVL) from the Guadalest Valley in Spain and known to differ in plasmid content (i.e., plasmids pXF64-Hb_ESVL of 59,678 bp and pUCLA-ESVL of 1,289 bp were present in ESVL only) (Giampetruzzi et al. 2019). Additionally, two strains of *X. fastidiosa* subsp. *multiplex* isolated from blueberry in Georgia and Florida (AlmaEm3 and BB08-1, respectively) and one *X. fastidiosa* subsp. *fastidiosa* strain from grapevines in California (TemeculaL), a variant of Temecula1 (Potnis et al. 2019), used in similar studies (Kandel et al. 2018; Wei et al. 2021) were used as reference strains for purposes of comparison with the Spanish strains (Table 1).

All strains were cultured from glycerol stocks on PD2 broth (Davis 1980) or modified PW agar (Davis et al. 1981) plates at 28°C in the dark. After 6 to 8 days, cells were re-streaked onto new plates and cultured for 5 days before using them in each experiment. Stocks of *X. fastidiosa* cultures were stored in PD3 broth plus 50% glycerol at −80°C. PD3 broth and agar (Davis et al. 1981) were used in all the experiments, except for the twitching experiments, in which PW agar without bovine serum albumin (BSA) was used (Galvani et al. 2007).

Growth, biofilm, and planktonic quantification and cell-to-cell aggregation assessment

Biofilm and planktonic growth for each strain was estimated by measuring the OD_{600} of cells grown in PD3 medium in polystyrene 96-well microplates (COSTAR, Kennebunk, ME, U.S.A.). At time 0, microplate wells were inoculated with 200 µl of a cell suspension on PD3 ($OD_{600} = 0.08$). The microplates were then incubated at 28°C with shaking (200 rpm) for 7 days. Wells filled with noninoculated PD3 served as controls. OD_{600} was measured daily using a Cytation 3 Image Reader spectrophotometer (BioTek Instruments, Winooski, VT, U.S.A.). Each measurement was corrected by subtracting values from control noninoculated wells; growth curves of the different strains were obtained by assessing accumulated growth over time. The standardized area under the growth progress curve (SAUGPC) was calculated using the trapezoidal integration method standardized by duration of the experiment in days (Simko and Piepho 2011). Ten wells (replications) per strain were included on each of the two microplates used per experiment, with a total of four independent experiments conducted.

In addition, at the end the experiment, total growth, planktonic growth, and biofilm formation were quantified using the crystal violet assay, as described previously (Zaini et al. 2009), with some modifications. Briefly, 150 µl of the cell suspension in each well was transferred onto a new plate to measure the planktonic growth. To determine biofilm formation, the original plate was rinsed with Milli-Q water, stained with 0.1% crystal violet at room temperature for 20 min, and rinsed again three times to remove all the unbound crystal violet, followed by the addition of 95% ethanol and agitation for 5 min. Planktonic growth and biofilm formation were measured by OD_{600} as described above. Ten wells (replications) per strain were included in two microplates per experiment, with a total of three independent experiments conducted.

Biofilm development was also assessed at the air-liquid interface of glass tubes to evaluate cells' auto-aggregation (Cruz et al. 2012; Li et al. 2007). For this assessment, glass tubes containing 3 ml of PD3 medium were inoculated with cell suspensions of each strain adjusted to $OD_{600} = 0.1$. Glass tubes were incubated at 28°C with agitation (200 rpm) for 8 days. Three replications for each strain were included in each experiment, with a total of four independent experiments performed. Cells from glass tubes were used to determine the settling rate, as a measure of cell-to-cell aggregation, as described before (Kandel et al. 2017), with some modifications. To do so, cell suspensions were homogenized in glass tubes

by vortexing, and 1 ml was transferred onto a polystyrene spectrophotometer cuvette (Labbox Labware, Barcelona, Spain). OD_{600} was measured using a UV-Vis 2450 spectrophotometer (Shimadzu Scientific Instruments, Columbia, MD, U.S.A.) at times 0 and 60 min. The settling rate was calculated when cells visually settled in the cuvettes (0 to 60 min postinoculation) using the following formula: {settling rate = $[\ln(OD_{600}(T0)) - \ln(OD_{600}(T60))]$/time}.

Growth and bacterial cell attachment in microfluidic chambers

To study the growth patterns and cell adhesion of ESVL and IVIA5901 strains, microfluidics chambers were used as an artificial model simulating xylem vessels. A TemeculaL strain was used for comparative purposes. The process of device fabrication was performed as previously described (De La Fuente et al. 2007a, 2008; Meng et al. 2005). Briefly, each microfluidic chamber consisted of two parallel microchannels (80 μm wide, 50 μm deep, and 3.7 cm long) on a polydimethylsiloxane surface bonded to a cover glass and a supporting glass microscope slide. Each microchannel had two inlets for the introduction of liquid media and bacterial suspension and an outlet for the collection of fluid flow. Before the introduction of bacterial cells, each connecting tube and microfluidic channel was flushed with two 5-ml plastic syringes (Hamilton Company, Reno, NV, U.S.A.) filled with PD3 broth medium. Cell suspensions (OD_{600} = 0.08) in PD3 broth for each strain were introduced into the microfluidic chamber with another pair of 1-ml plastic syringes (Becton Dickinson & Company, Franklin Lakes, NJ, U.S.A.). The flow of nutrient media and cell suspension was controlled with two programmable syringe pumps (Pico Plus; Harvard Apparatus, Holliston, MA, U.S.A.). First, the flow rate of media was maintained at 1 μl min^{-1} for 1 h to stabilize the system; after that, the cell suspension was introduced at a flow rate of 1 μl min^{-1}. Once enough cells were attached to the glass substrate inside the microchannel, the flow rate was adjusted to 0.25 μl min^{-1}. Time-lapse images were acquired every 30 s for a period between 10 and 14 days.

Adhesion force was assessed using microfluidic chambers as describe before (De La Fuente et al. 2007b). When enough cells were attached to the glass surface, media flow was maintained at 0.1 to 1 μl min^{-1} for 60 min to remove nonattached cells. After that, media flow was sequentially increased from 2 to 10 min^{-1} for the first minute and increased in steps of 10 μl min^{-1} every minute until a flow of 160 μl min^{-1} was reached. For these experiments, time-lapse images were acquired every 5 s for 16 min, and the number of attached cells in each frame was counted. The adhesion force of IVIA5901, ESVL, and TemeculaL strains was assessed by calculating the fraction of cells that detached from the glass substrate as a function of the total force required to remove them (De La Fuente et al. 2007b). The experiments were repeated at least four times for each strain. In each microfluidic chamber, the ESVL strain was used in one of the channels and compared with IVIA5901 or TemeculaL. Microfluidic chambers, in both types of experiment, were monitored under a 40× objective on a Nikon Eclipse Ti inverted microscope (Nikon, Melville, NY, U.S.A.), using Nomarski differential interference contrast optics and phase contrast. Time-lapse images were acquired using a Nikon DS-Q1 digital camera controlled by NIS-Elements Advanced Research 3.01 (Nikon), and the NIS-Elements imaging software version 3.0 was used to count the number of cells and combine the time-lapse images.

Quantification of twitching motility on agar plates and microfluidic chambers

Colonies from each strain were picked with a loop and gently spotted onto the surface of PW agar without BSA. Plates were incubated at 28°C for 5 days, and the peripheral fringe width of the colonies was observed after 2 and 5 days under 10× magnification using a Nikon DS-Q1 digital camera connected to a Nikon Eclipse Ti inverted microscope (Meng et al. 2005). The edge morphology of each colony was determined in six colonies per strain, and fringe width was measured three times per colony using the software Image–J2/Fiji (Rueden et al. 2017). Three independent experiments were performed.

Additionally, the twitching speed of ESVL and TemeculaL strains was assessed in microfluidic chambers as previously described (Cruz et al. 2012; Meng et al. 2005), with some modifications. The cell motility speed of ESVL cells was compared with that of the TemeculaL strain, which has been described to show high cell motility (De La Fuente et al. 2007a). The IVIA5901 strain was not included due to the lack of motility observed in previous microfluidic experiments. When twitching was observed, time-lapse images were acquired every 30 s for 2 or 3 h, and tracking of bacterial cell positions was quantified using the software Image–J2/Fiji (Rueden et al. 2017). Cell speed was calculated by measuring the upstream movement of cells frame by frame over time. Five measurements per strain and experiment were collected, and three independent experiments were performed.

Transmission electron microscopy

To determine the presence of type I and type IV pili, we used transmission electron microscopy (TEM) following a previously described protocol by Kandel et al. (2017), with some modifications. Cell suspensions from ESVL and IVIA 5901 strains were obtained by scrapping bacterial cells from the peripheral fringe of 4-day-old colonies grown on PD2 agar plates that were resuspended in 200 μl of sterile water. The TemeculaL strain was used for comparative purposes. Ten microliters of the cell suspension was deposited on 300-mesh carbon-coated copper grids (Electron Microscopy Sciences, Hatfield, PA, U.S.A.). The cells were allowed to settle for 10 min, and then the leftover liquid was blotted out carefully with a filter paper. After that, the grid was negatively stained with 10 μl of phosphotungstic acid for 2 min and observed with a TEM JEM-1400 (Jeol, Tokyo, Japan) at the electron microscopy facilities of the Central Research Support Services of the University of Córdoba (UCO-SCAI, Spain). The lengths of 99 cells, 33 pili type I, and 66 pili type IV were measured using the open source analysis software Image–J2/Fiji (Rueden et al. 2017).

Virulence assessment

The virulence of the five strains was evaluated using tobacco (*Nicotiana tabacum*) cultivars Petite Havana SR1 and Xanthi, as previously described (De La Fuente et al. 2013). Three-week-old seedlings were transplanted into 11.5-cm square pots with Sunshine Mix #8 substrate (Sun Gro Horticulture Canada Ltd., Vancouver, Canada). Plants were grown in a greenhouse at 20 to 25°C with nat-

TABLE 1. Characteristics of *Xylella fastidiosa* strains used in this study

Subspecies/strain	Host plant	Place of isolation (year)	Sequence type	Reference
subsp. *multiplex*				
IVIA5901	*Prunus dulcis*	Bolulla, Alicante, Spain (2017)	6	(Giampetruzzi et al. 2019)
ESVL	*Prunus dulcis*	Benimantell, Alicante, Spain (2017)	6	(Giampetruzzi et al. 2019)
BB08-1	*Vaccinium* sp.	Putnam, Palatka, Florida, U.S.A. (2008)	43	(Oliver et al. 2014; O'Leary et al. 2022)
AlmaEm3	*Vaccinium* sp.	Alma, Bacon, Georgia, U.S.A. (2011)	42	(Oliver et al. 2014; O'Leary et al. 2022)
subsp. *fastidiosa*				
TemeculaL	*Vitis vinifera*	Temecula, Riverside, California, U.S.A. (1998)	1	(Kandel et al. 2018; Potnis et al. 2019)

ural sunlight for 5 months, watered regularly, and fertilized every 6 weeks with Osmocote (outdoor and indoor smart-release plant food; The Scotts Company, Marysville, OH, U.S.A.). Tobacco plants were inoculated at the five-to-six true-leaf stage (3 weeks after transplanting). The upper part of the plant was cut, leaving only the lowest two or three true leaves. For inoculation, 20 µl of a cell suspension in succinate-citrate-phosphate buffer (PBS) at an initial OD_{600} = 0.8 concentration was inoculated at the leaf petiole (two leaves per plant). It was then pricked several times with a sterile entomological needle until the cell suspension was absorbed by the plant. A second inoculation was performed 1 week later, following the same procedure. Nine plants were inoculated for each of the AlmaEm3, BB08-1, ESVL, IVIA5901, and TemeculaL strains. Control plants were inoculated using the same procedure but using PBS instead of a cell suspension. Plants were evaluated periodically for the appearance of disease symptoms (yellowing, leaf curling, and leaf scorch symptoms). After the first visible symptoms appeared, the disease incidence and severity were estimated by the percentage of leaves showing disease symptoms at weekly intervals. Data on symptom severity were plotted over time to obtain disease severity progress curves that were used to calculate the area under the disease severity progress curves standardized by the duration of disease development in days (SAUDPC) (Simko and Piepho 2011). Two independent experiments were conducted.

Comparative genome analysis

The completed circularized genome of the ESVL strain was obtained by following a similar approach as previously described (Arias-Giraldo et al. 2020). An Oxford Nanopore technology sequencing library was prepared using the transposase-based rapid sequencing kit following the manufacturer's recommendations and generated in-house using an R9.4 flow cell with the MinION device. The ESVL strain library was multiplexed equimolarly in the same flow cell with the other 11 *X. fastidiosa* strains. The multiplexed library was sequenced in a standard run protocol of 48 h. The preprocessing of the raw data generated by MinION, which includes the filtering and trimming steps, was performed with Filtlong v0.2.0 (https://github.com/rrwick/Filtlong) and Porechop v0.2.3 (https://github.com/rrwick/Porechop), removing adapters and reads shorter than 2 kb. A draft assembly was obtained using Flye v2.7.1 (Kolmogorov et al. 2019) that was then polished in two rounds with the Illumina short reads obtained in a previous study (Giampetruzzi et al. 2019) using the POLCA tool (Zimin and Salzberg 2020). The bacterial chromosome was reoriented using a Circlator v1.5.5 bioinformatic tool (Hunt et al. 2015), setting the *dna*A gene as the starting point. The complete circularized genome of the ESVL strain has been deposited in the GenBank genome database under accession number CP099516.

The complete circularized genome of IVIA5901 was retrieved from the NCBI GenBank database (assembly accession GCA_004023395.2) (Arias-Giraldo et al. 2020). For functional annotation and classification using subsystems, polished assemblies were submitted to the RAST (Rapid Annotation using Subsystem Technology) server (Aziz et al. 2008; Brettin et al. 2015) and compared and visualized using the SEED viewer (Overbeek et al. 2014). To evaluate the similarities of the genomes and the nucleotide sequence homology of the predicted coding DNA sequences (CDSs) between the two close Spanish strains, all-versus-all bidirectional BLAST hits were calculated using the RAST server platform. Protein encoding sequences with 100% identity were discarded in order to find out the unique CDSs of each strain. Genome alignment and single-nucleotide polymorphism (SNP) positions in the chromosomes for both strains were computed using the progressive MAUVE algorithm v2.4.0 (Darling et al. 2004) with default parameters.

Additionally, an approach similar to that of D'Attoma et al. (2020) was used to perform a comparison of gene sequences and amino acid sequence variation for (i) the CDSs that showed SNPs after MAUVE analysis and (ii) genes identified in previous studies potentially related to adhesion and aggregation functions and twitching motility (*pilA1*, *pilB*, *pilM*, *pilN*, *pilQ*, *pilO*, *pilT*, *pilY1*, *recA*, *comA*, and *comF*). The comparison was made between sequences of ESVL and IVIA5901 strains, in addition to each of them being compared with the genome of the reference strain Temecula1 (NC_004556.1) retrieved from the GenBank database. Amino acid sequence variations were compared using an EMBOSS Needle pairwise sequence alignment tool and a dot-plot tool (EMBOSS Dotmatcher) (Madeira et al. 2019). The impact of each amino acid variation on the biological function of the studied proteins was predicted using the PROVEAN (Protein Variation Effect Analyzer; JCVI, La Jolla, CA, U.S.A.) web server (Choi and Chan 2015), with a default cutoff value of −2.5. Amino acid variations with a PROVEAN score equal to or below this threshold were considered deleterious and potentially having an influence on the biological function of that protein, whereas if the value was higher than the threshold, it was classified as neutral.

Statistical analyses

X. fastidiosa strain parameters (i.e., growth rate, biofilm formation, settling rate, twitching motility, and virulence) were analyzed using standard analysis of variance (ANOVA) with a randomized complete block design in which blocks represented the experiment runs and the strain was the main factor. For the virulence tests, the SAUDPC was analyzed using a factorial design, with *X. fastidiosa* strain and tobacco cultivar being the two main factors. In all cases, ANOVA assumptions were evaluated by testing for normality and homoscedasticity using the Shapiro-Wilk test, Bartlett's test, and normal q-q plots. If those assumptions were violated, the Box-Cox transformation was applied to the data (Sakia 1992). Post hoc Tukey's honestly significant difference test at $P < 0.05$ was used for pairwise means comparison among main factor levels. In addition, a paired *t* test with Bonferroni correction was performed to compare the SAUDPC values between the two Spanish strains.

All statistical tests and analyses were perform using R software version 3.6.2 (R Core Team 2020) using R packages "agricolae" v. 1.3-3 (de Mendiburu 2020) and "MASS" v. 7.3-51.4 (Venables and Ripley 2013). All the experiments were repeated at least two times.

Results

Growth, biofilm formation, cell-cell aggregation, and adhesion force

In general, the bacterial growth of all strains reached a stationary phase after ∼144 h of incubation (Fig. 1A). Total growth, estimated by the SAUGPC, was significantly the highest ($P < 0.05$) for the IVIA5901 (0.054 ± 0.004) and AlmaEm3 (0.055 ± 0.004) strains, intermediate ($P < 0.05$) for TemeculaL (0.043 ± 0.003), and lowest ($P < 0.05$) for ESVL (0.027 ± 0.002) and BB08-1 (0.029 ± 0.005) (Fig. 1B). When comparing the two Spanish strains, the SAUGPC was significantly higher ($P < 0.05$) for IVIA5901 than for ESVL (Fig. 1B).

The biofilm formation and planktonic growth of *X. fastidiosa* strains were determined at the end of the experiment by measuring OD_{600} (Figure 1C and D). The biofilm formation was highest ($P < 0.05$) for the BB08-1 (0.322 ± 0.024) and AlmaEm3 (0.281 ± 0.022) strains and intermediate ($P < 0.05$) for TemeculaL (0.169 ± 0.010), and the smallest biofilm formation ($P < 0.05$) was observed for IVIA5901 (0.051 ± 0.005) and ESVL (0.042 ± 0.004) (Fig. 1B). Planktonic growth was highest ($P < 0.05$) for TemeculaL and IVIA5901 and intermediate ($P < 0.05$) for ESVL, and the smallest growth ($P < 0.05$) occurred for BB08-1 and AlmaEm3 (Fig. 1D). When compared with the three reference strains used here, the Spanish IVIA5901 and ESVL strains showed the lowest values ($P < 0.05$) for biofilm formation (Fig. 1C) and reached the highest (IVIA5901) and intermediate (ESVL) levels of planktonic growth (Fig. 1D) or highest (IVIA5901) and low-

est (ESVL) levels of total growth as measured by the SAUGPC (Fig. 1B).

Formation of biofilm on glass tubes showed differences among the five *X. fastidiosa* strains included in the study. The IVIA5901 and ESVL strains exhibited a reduced ring of biofilm in the water/air interface compared with that formed by the reference strains TemeculaL, AlmaEm3, and BB08-1 (Fig. 2A). In addition, whereas bacterial aggregates were observed at the bottom of the tubes for the AlmaEm3, BB08-1, and TemeculaL strains, IVIA5901 and ESVL showed a turbid growth, indicating that both strains were impaired in their ability to form aggregates in PD3 liquid culture and that they grow mainly in the planktonic phase. In accordance with these results, cell settling rates, as a measure of cell-cell aggregation (reduction of OD_{600}/min), were much lower ($P < 0.05$) for the IVIA5901 (0.0004 ± 0.0002) and ESVL (0.0002 ± 0.0001) strains as compared with those reached by the BB08-1 (0.0054 ± 0.0018), AlmaEm3 (0.0050 ± 0.0016), and TemeculaL (0.0047 ± 0.0008) strains, which showed a cell aggregation capacity at least 16 times higher than that of both Spanish strains (Fig. 2B).

Cell aggregation was also assessed under flow conditions for the TemeculaL, IVIA5901, and ESVL strains using microfluidic chambers (Fig. 3A). TemeculaL showed a higher aggregation than the Spanish strains, with large aggregates of cells being formed at 4 days postinoculation (dpi), which occupied a major part of the surface of the channel at 8 dpi. For the ESVL strain, cells were attached to each other, forming lace-like masses after 1 and 4 dpi, with small cell aggregates observed in several sections of the microchannel at 4 dpi (Fig. 3A). Some aggregates increased in size,

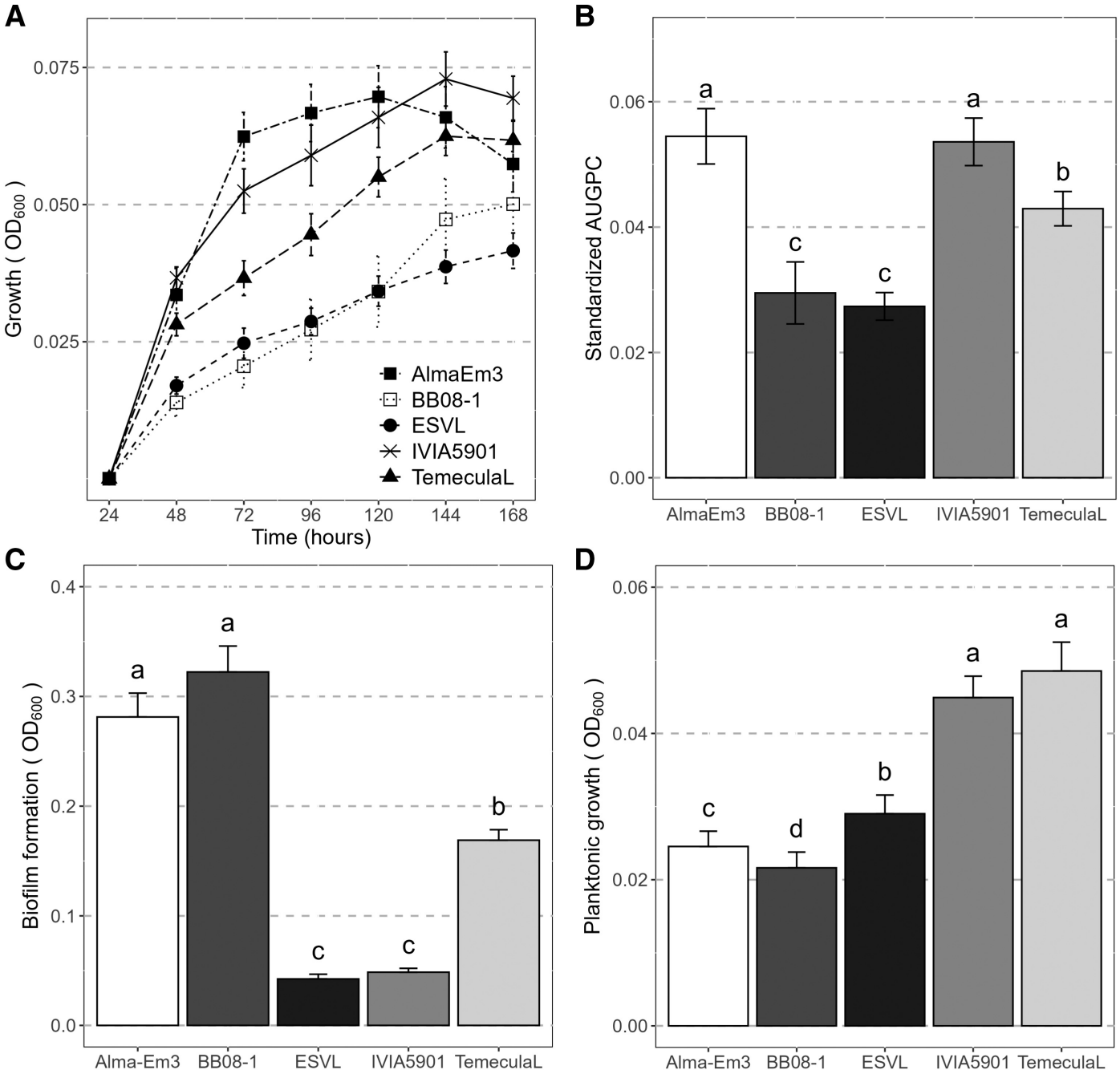

Fig. 1. Phenotypic characterization of bacterial growth in vitro. **A,** Growth curves; **B,** standardized area under growth progress curves (SAUGPC); **C,** biofilm formation; and **D,** planktonic growth for *Xylella fastidiosa* strains grown at 28°C in 96-well plates for 7 days. Each point in panel A and bar in panels B, C, and D represents the mean value of three independent experiments under the same conditions. Vertical lines represent the standard error of the mean. Bars with different letters indicate significant differences ($P < 0.05$) according to a post-hoc protected Tukey's honestly significant difference test.

but aggregates were not longer than 20 μm. In contrast, although some small aggregates could also be observed for the IVIA5901 strain at 4 dpi, the number and size of the aggregates were smaller compared with those of ESVL (Fig. 3A).

Finally, adhesion force, which refers to the amount of force necessary for cell detachment from surfaces, was determined for the two Spanish strains and TemeculaL using microfluidic chambers (Fig. 3B and C; Supplementary Video S1). Detachment of cells was observed when the flow rate was higher than 40, 30, and 20 μl min^{-1} for the ESVL, IVIA5901, and TemeculaL strains, respectively (Fig. 3B). At a higher flow rate, the number of attached cells decreased rapidly, showing a linear trend with the increase in the flow rate, with a rate of detachment significantly ($P < 0.05$) lower for ESVL (-0.64 ± 0.03 to 0.70 ± 0.03), followed by IVIA5901 (-0.81 ± 0.07). The reference strain TemeculaL had the highest ($P < 0.05$) rate of detachment (-1.15 ± 0.06) (Fig. 3B). The average adhesion force was estimated at 396.77 ± 12.77 pN for ESVL, which was significantly ($P < 0.05$) higher than those observed for IVIA5901 (272.76 ± 22.61 pN) and TemeculaL (219.67 ± 8.44 pN) (Fig. 3C), indicating a higher attachment capacity for the ESVL strain.

Twitching motility

In general, at 1 to 3 dpi, individual cells of ESVL showed a minimal ability to move against the flow of liquid medium, whereas no movement against the flow was observed for cells of the IVIA5901 (Supplementary Video S2) strain. However, when compared with TemeculaL, only a few cells of ESVL could move against the flow, whereas most of the cells of the TemeculaL strain showed this ability. The twitching speed motility of ESVL was quantified, and it was significantly ($P < 0.05$) lower at 0.33 ± 0.02 μm min^{-1} compared with 0.41 ± 0.01 μm min^{-1} for TemeculaL cells (Supplementary Video S3).

To determine twitching motility in more detail, the fringe width of bacterial colonies growing on PW agar without BSA was measured. Colonies were designated as twitch positive when a fringe was observed on the colony. A peripheral fringe was detected for all studied strains, except for IVIA5901, which showed no visible peripheral fringe within the 5 days of incubation (Fig. 4A). For the four remaining strains, the peripheral fringe varied among them and depending on the observation time (Fig. 4B). The AlmaEm3, BB08-1, and TemeculaL strains showed a peripheral fringe at 2 and 5 days, whereas for ESVL, it was observed only after 2 days, not being observed at 5 days of incubation (Fig. 4B), probably due to overgrowth of the bacterial colony. This behavior was consistently observed for all replicated experiments. At 2 days of incubation, the peripheral fringe width ranged from 8.23 ± 1.67 to 18.99 ± 2.17 μm for the BB08-1 and ESVL strains, respectively (Fig. 4B), whereas at 5 days of incubation, the length of the peripheral fringe was estimated at 17.51 ± 1.42 to 18.29 ± 1.71 μm for the AlmaEm3 and BB08-1 strains, respectively (Fig. 4B). TemeculaL showed the widest peripheral fringe ($P < 0.05$), at 31.04 ± 2.07 and 83.28 ± 4.47 μm after 2 and 5 days of incubation, respectively (Fig. 4B).

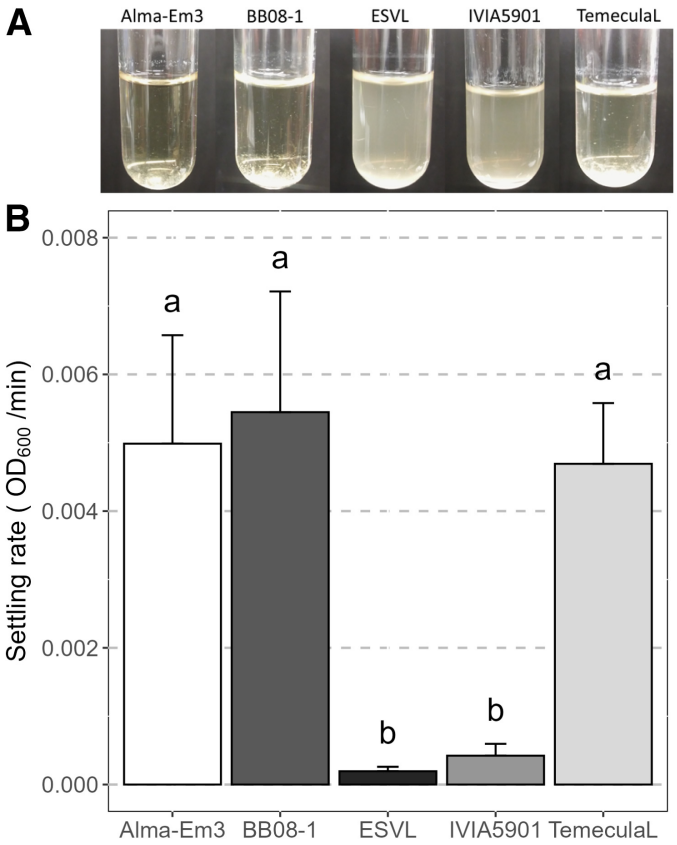

Fig. 2. Adhesion phenotypes in vitro. **A,** Biofilm formation by *Xylella fastidiosa* strains studied on glass surfaces grown at 28°C for 8 days. **B,** Settling rates of *X. fastidiosa* strains as a measure of cell-to-cell aggregation. Each bar represents the mean value of four independent experiments under the same conditions. Vertical lines represent the standard error of the mean. Bars with different letters indicate significant differences ($P < 0.05$) according to a post-hoc protected Tukey's honestly significant difference test.

Presence of pili in ESVL and IVIA5901 cells by TEM imaging

TEM imaging allowed for the observation of type I and IV pili in the cells of both Spanish strains (ESVL and IVIA5901) and in the control strain TemeculaL (Fig. 5). Abundant short type I pili were detected in all strains, with a similar length ($P \geq 0.05$) among them, estimated at 0.44 ± 0.02 and 0.44 ± 0.03 μm in the ESVL and IVIA5901 strains, respectively, whereas for TemeculaL, the type I pili length was 0.42 ± 0.03 μm (Supplementary Fig. S1A). Similarly, the length of type IV pili showed no significant ($P \geq 0.05$) differences among strains, estimated at 3.48 ± 0.54 and 3.45 ± 0.65 μm in the ESVL and IVIA5901 strains, respectively, whereas for TemeculaL, the type I pili length was 4.44 ± 1.33 μm (Supplementary Fig. S1B). Cell length varied among strains ($P < 0.05$), estimated at 1.26 ± 0.07 μm for IVIA5901 and 1.59 ± 0.07 μm for ESVL, and it was highest for TemeculaL, with a cell length of 1.87 ± 0.06 μm (Supplementary Fig. S1C).

Virulence assessment

The AlmaEm3, BB08-1, ESVL, IVIA5901, and TemeculaL strains were able to infect and induce disease symptoms in both tobacco cultivars used: Petite Havana SR1 and Xanthi. The first symptoms were observed within 100 to 110 days after inoculation in plants inoculated with the AlmaEm3 and TemeculaL strains, whereas plants inoculated with ESVL and IVIA5901 showed their first symptoms 1 or 2 weeks later. Symptoms consisted of yellowing, leaf curling, and leaf scorch.

Overall, disease severity on the two tobacco cultivars progressed following a linear trend over time (Fig. 6A and B). The disease outcome estimated by the SAUDPC was mainly influenced by the strain ($P < 0.05$), with a nonsignificant effect ($P \geq 0.05$) of the tobacco cultivar or the interaction between both factors. Irrespective of the tobacco cultivar, the SAUDPC was significantly higher ($P < 0.05$) for the TemeculaL and AlmaEm3 strains, reaching, respectively, values of 39.71 ± 4.29 and 32.01 ± 5.45 for Petite Havana SR1 and 40.94 ± 4.74 and 30.17 ± 5.71 for Xanthi compared with the other three strains, which showed no significant differences ($P \geq 0.05$) among them. However, the BB08-1 and ESVL strains did not differ significantly from AlmaEm3 or IVIA5901 (Fig. 6C). For these strains, the SAUDPC ranged from 7.09 ± 2.11 for IVIA5901 to 18.13 ± 3.44 for BB08-1 on Petite Havana SR1 and from 10.31 ± 1.81 for IVIA5901 to 18.10 ± 4.11 for ESVL on Xanthi (Fig. 6C). For both cultivars, the Spanish strains ESVL and IVIA5901 reached a significantly lower ($P < 0.05$) disease development compared with TemeculaL and AlmaEm3 (only strain IVIA5901), but it was

similar to that reached by the BB08-1 strain (Fig. 6C). Moreover, no significant differences ($P > 0.55$) were observed between the SAUDPC values of the two Spanish strains when compared by a paired test.

Comparative genome analysis

The RAST server annotation process identified a total of 2,857 CDSs for the IVIA5901 strain and 2,929 CDSs for the ESVL strain. The genomic features of both strains are summarized in Table 2. In ESVL, the pUCLA-ESVL plasmid only contains one CDS for a replication protein (849 bp). The plasmid pXF64-Hb_ESVL contains 59 CDSs, including nine plasmid conjugative transfer proteins (Tra-H, I, M, N, O, Q, T, U, and W), two conjugative transfer proteins (TrbB and TrbN), two plasmid conjugative transfer DNA primases, four chromosome (plasmid) partitioning proteins (ParA [three copies] and ParB), two transcriptional regulators, two flagellar hook-length control proteins (FliK), two helicases, one twitching motility protein (PilT), one MobD protein, one MobA protein, one DNA topoisomerase, one mobile element protein, one transposase (OrfB), one predicted kinase, one DNA primase (DnaG), one in-

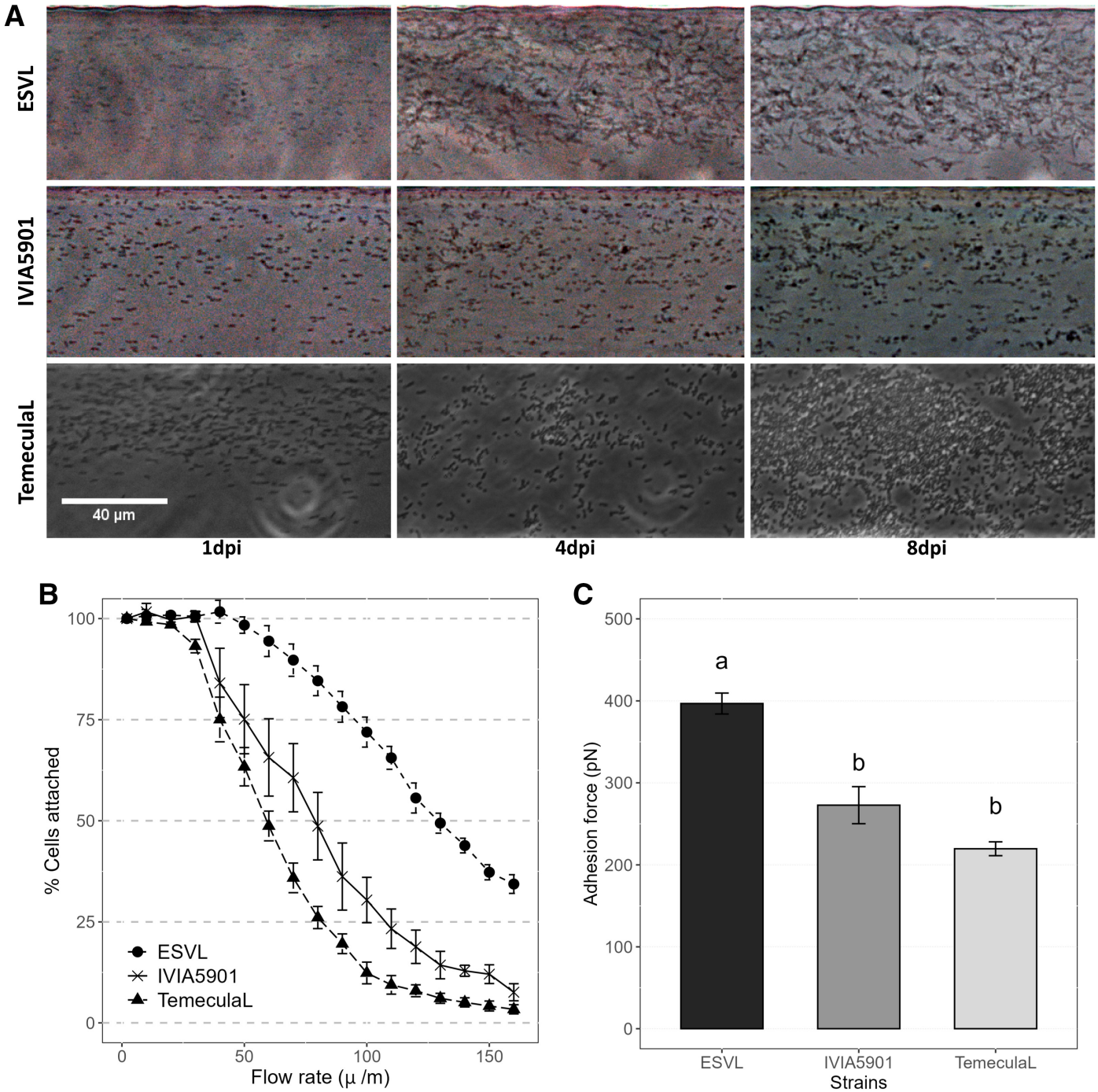

Fig. 3. Phenotypic characterization in microfluidic chambers. **A,** Time-lapse micrographs showing the formation of cell aggregates in microfluidic chambers for *Xylella fastidiosa* strains ESVL (upper panels), IVIA5901 (middle panels), and TemeculaL (lower panels). Images in each column were captured at 1, 4, and 8 days postinoculation (left to right). Scale bar is shown in the bottom left image. **B,** Percentage of cell surface attachment measured inside microfluidic chambers with increasing medium flow rate. **C,** Adhesion force, measured in piconewtons (pN), of cells of *X. fastidiosa* strains ESVL, IVIA5901, and TemeculaL. Each point or bar represents the mean value of four independent experiments under the same conditions. Vertical lines represent the standard error of the mean. Bars with different letters indicate significant differences ($P < 0.05$) according to a post-hoc protected Tukey's honestly significant difference test.

tegral membrane protein, one outer membrane lipoprotein-sorting protein, one single-stranded DNA-binding protein, one permease component of a branched-chain amino acid ABC-type transport system, one synthase or enzyme-like protein precursor, and 23 hypothetical proteins (Fig. 7B; Supplementary Table S1).

The MAUVE genome alignment of both Spanish strains revealed a good synteny and identified four locally collinear blocks that are different homology regions in each strain (Fig. 7A). A small rearrangement of a region of 9,050 bp (from the 631,461 to 640,511 bp position in IVIA5901 and from the 954,252 to 963,302 bp position in ESVL) was found. In this chromosomal region, we found a cluster of CDSs related to phages (Fig. 7A).

A total of 2,672 CDSs were shared between both strains; however, some differences were found. A total of 85 unique CDSs were identified in the chromosome of the IVIA5901 strain, of which 78 were hypothetical proteins and seven were

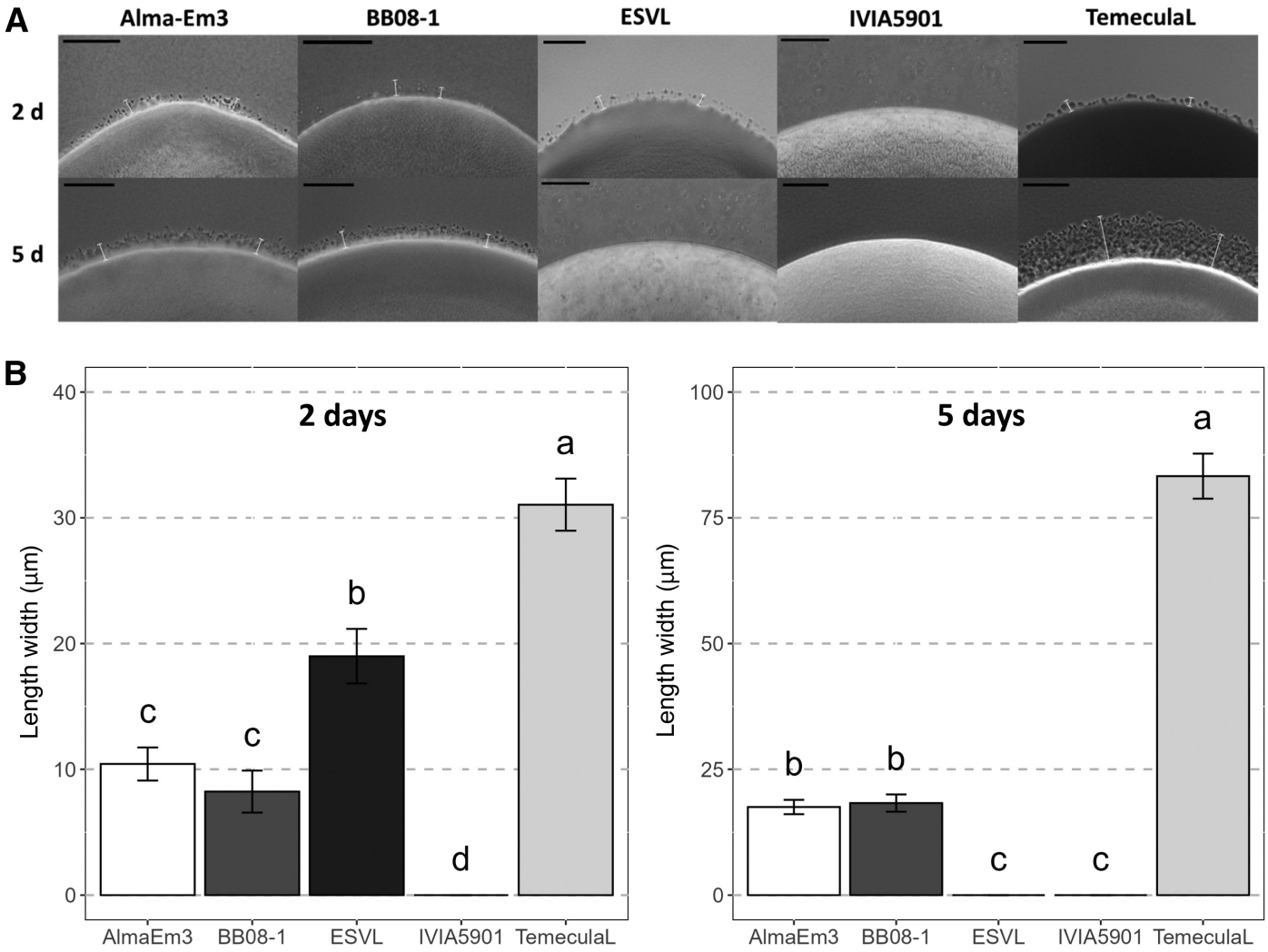

Fig. 4. Twitching motility assessment. **A,** Colony morphology (scale bar, 100 µm) and **B,** measurements of colony fringe widths of *Xylella fastidiosa* strains on the surface of modified PW without bovine serum albumin agar, after 2 (left panel) and 5 (right panel) days of incubation at 28°C. Each bar represents the mean value of three independent experiments under the same conditions. Vertical lines represent the standard error of the mean. In each panel, bars with different letters indicate significant differences ($P < 0.05$) according to a post-hoc protected Tukey's honestly significant difference test.

TABLE 2. Genomic features of the completed circularized genome of *Xylella fastidiosa* subsp. *multiplex* IVIA5901 and ESVL strains

	X. fastidiosa subsp. *multiplex* IVIA5901	*X. fastidiosa* subsp. *multiplex* ESVL		
Features	Chromosome	Chromosome	Plasmid pXF64-Hb_ESVL	Plasmid pUCLA-ESVL
Genome size (bp)	2,559,117	2,552,692	59,660	1,289
GC content (%)	52	52	…	…
Contigs	1, circular	1, circular	1, circular	1, circular
Total features	3,021	3,022	63	1
Coding DNA sequences (CDSs)	2,857	2,869	59	1
RNAs	54	54	…	…
Repeated regions	101	90	4	…
Prophages	9	9	…	…
Subsystems	227	228	…	…
CDSs in subsystems	864	836	…	…
CDSs with assigned function (no hypothetical)	1,780	1,794	36	1
Potential missing genes	8	7	…	…

a glutamine-fructose-6-phosphate aminotransferase, a DsbA-like thioredoxin domain, a glycosyl transferase, an LSU ribosomal protein (L36p), a RelB/StbD replicon stabilization protein (antitoxin to RelE/StbE), an mRNA interferase RelE protein, and a dipeptidyl aminopeptidases/acylaminoacyl-peptidase (Fig. 7B; Supplementary Table S2). On the other hand, 85 unique CDSs were found in the ESVL strain chromosome, of which 76 were hypothetical proteins, three were DNA helicase phage-associated, one was a phage-related protein, one was an alpha-2-macroglobulin, one was a large exoprotein involved in heme utilization or adhesion, one was a hemagglutinin-like secreted protein, one was a polygalacturonase (EC 3.2.1.15), and one was a PE_PGRS (wag22) (Fig. 7B; Supplementary Table S3). Of the 59 CDSs present in the pXF64-Hb_ESVL plasmid annotated by the RAST server, 50 have been identified as unique to the ESVL strain (Fig. 7B; Supplementary Table S3), and the remaining nine have shown some degree of similarity to CDSs in the chromosome of the IVIA5901 strain, including the protein PilT, related to twitching motility (Fig. 7B; Supplementary Table S4). The only CDS of pUCLA-ESVL was not found in IVIA5901.

Finally, a total of 376 SNPs were identified in the chromosome when comparing the genomes of both Spanish strains. Of these SNPs, 321 are in CDSs encoding for proteins, and the remaining features are prophages, repeated sequences, or RNA or are detected in noncoding regions. Interestingly, almost 96% of these CDSs are phage-related or hypothetical proteins (Supplementary Table S5). The rest of the CDSs with SNPs include six encoding proteins predictably involved in bacterial adhesion or in other traits involved in pathogenicity: a phosphoserine phosphatase, a hemolysin-type calcium-binding protein, a mobile element protein, two large exoproteins involved in heme utilization and/or adhesion of the IVIA5901 strain (fig|2371.581.peg.1315, fig|2371.581.peg.2413), and an autotransporter adhesin (Supplementary Table S5) that showed either a punctual mutation or was fragmented or divided into several proteins in the ESVL strain. However, none of these amino acid variants was predicted to be potentially deleterious by PROVEAN tool (Supplementary Table S6).

When comparing the CDSs that showed variant SNPs between both Spanish strains with those of the reference genome of the Temecula1 strain, we observed that the homologous *pspA* gene in the Temecula1 genome contains a frameshift (PD_1732 and PD_0988). The other CDSs, with the exception of the phosphoserine phosphatase, had percentages of identity ranging from 64.8 to 84.1%, similarity (32.3 to 86.1%), and gaps (2.4 to 32.2%) according to pairwise global alignments, showing a different length, with a large number of SNPs and deletions and insertions of different amino acids, which in some cases resulted in a truncated organization or were divided into several proteins.

Finally, PROVEAN comparison analysis of selected adhesion-, aggregation-, and twitching-related genes (*pil*A1, *pil*B, *pil*M, *pil*N, *pil*Q, *pil*O, *pil*T, *pilY1*, *rec*A, *com*A, and *com*F) revealed no amino acid differences between the ESVL and IVIA5901 strains. However, three SNPs were predicted to be deleterious for the *pilB*, *pilY1*, and *comF* genes in both Spanish strains when compared with the Temecula1 strain (Supplementary Table S6).

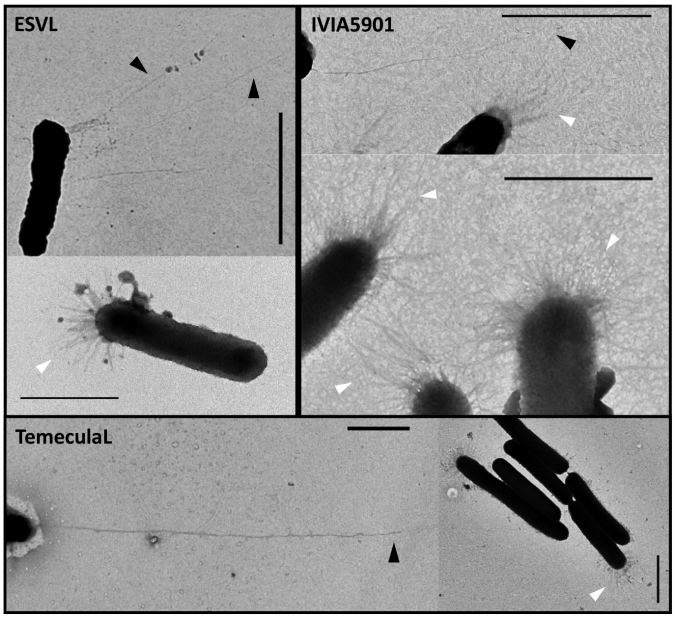

Fig. 5. Transmission electron micrographs of negatively stained cells of *Xylella fastidiosa* strains ESVL, IVIA5901, and TemeculaL. Black arrows indicate type IV pili, and white arrows indicate type I pili. Scale bar, 1 μm.

Discussion

In this study, we characterized traits related to the colonization and virulence of two *X. fastidiosa* strains (ESVL and IVIA5901) isolated from almond trees growing in the outbreak area of Guadalest Valley in the province of Alicante, Spain. Both strains were isolated in the same year, from the same plant species host, and from regions in Spain less than 16 km apart. Despite the high genetic similarity between the two Spanish strains (99% average nucleotide identity), important phenotypic (Table 3) and genomic differences were found when comparing both circularized genomes and the CDSs present in the two plasmids (Table 2; Supplementary Tables S1 to S6). The presence of two plasmids in the ESVL strain (pXF64-Hb_ESVL and pUCLA-ESVL) provided 51 unique CDSs. In addition, the genome analysis revealed the presence of unique CDSs and SNPs on both chromosomes that could affect adhesion, motility, cell wall degradation, the toxin-antitoxin system, and the development of outer membrane proteins, which might explain the differences found here in phenotypic traits (Table 3) associated with virulence.

The role of plasmids in the *X. fastidiosa* life cycle is still poorly understood, even though plasmids may contribute to virulence, epidemiology, and adaptation to new hosts and environments (Sengupta and Austin 2011). To date, 61 plasmids have been described in 38 *X. fastidiosa* strains from different geographical origins and host plants (Pierry et al. 2020), but no studies have determined the role of those plasmids in *X. fastidiosa* virulence. The large plasmid found in the ESVL strain (pXF64-Hb_ESVL) had a highly similarity (96.6% nucleotide identity) to the plasmid pXF64_HB found in *X. fastidiosa* subsp. *pauca* strain Hib4 (ST70) isolated from hibiscus. Both of those plasmids also share more than 80% nucleotide identity and over 57 to 71% length coverage with plasmids belonging to the genera *Xanthomonas*, *Paraburkholderia*, and *Burkholderia* (Pierry et al. 2020). On the other hand, the small plasmid (pUCLA-ESVL) was classified as nonmobilizable, showing high identity to three plasmids (pUCLA from the UCLA strain, pXF686 from the ATCC 35868 strain, and pXFPD1.3 from the Temecula1 strain) identified in strains of *X. fastidiosa* subsp. *fastidiosa* (Pooler et al. 1997; Simpson et al. 2000) isolated from grapevines. Previous research demonstrated experimentally that the presence of a type IV secretion system, encoded by *tra* and *trb* genes, similar to those present in the large plasmid of the ESVL strain, is responsible for the transfer of plasmids via conjugation (Burbank and Van Horn 2017). Transfer of plasmids can occur among subspecies and strains (Burbank and Van Horn 2017; Giampetruzzi et al. 2016; Hendson et al. 2001; Rogers and Stenger 2012). Moreover, it has been suggested that interspecies genetic exchange with other bacteria can occur (Burbank and Van Horn 2017; Denancé et al. 2019; Stenger et al. 2010), which may increase the possibility of acquiring beneficial new genetic material for the adaptation of *X. fastidiosa* to different host plants or environments.

Compared with the reference strains, ESVL and IVIA5901 showed less capacity for cell aggregation and biofilm formation. Detected mutations affected three proteins: an autotransporter adhesin,

a large exoprotein, and a hemolysin (Supplementary Table S6) with a high level of similarity to sequences encoding for afimbrial adhesins in the Temecula1 strain (Chen and De La Fuente 2020; Parker et al. 2016; Wang et al. 2012; Zhang et al. 2015). These proteins have been described as playing a main role in the process of biofilm formation and cell-to-cell aggregation in *X. fastidiosa* (Guilhabert and Kirkpatrick 2005; Killiny and Almeida 2009). Indeed, the CDSs for the three large exoproteins involved in heme utilization from the IVIA5901 strain showed a high similarity to those of Temecula1 (HxfA and HxfB). In contrast, the CDSs for the same protein in the ESVL strain showed a truncated organization, which generated two CDSs annotated as PE_PGRS (wag22) and a hemagglutinin with a high similarity to fragments of the *hxfB* gene. The presence of nucleotide frameshifts in large hemagglutinin proteins (*hxf* genes) were also reported in the *X. fastidiosa* subsp. *pauca* 'De Donno' strain, which is highly virulent in olive trees. It was suggested that the mutation of those genes might be related to the severe symptoms observed in different olive cultivars in Italy (Saponari et al. 2018). Indeed, *prtA*, *rpfC*, and *HxfA*-*HxfB* mutants of the Temecula1 strain showed lower aggregation, biofilm, and cell attachment than their wild types in susceptible grapevines (Gouran et al. 2016; Guilhabert and Kirkpatrick 2005; Newman et al. 2004). These phenotypes facilitate a higher number of cells colonizing the entire host plant (de Souza et al. 2020; Roper et al. 2019). Thus, the high number of planktonic cells observed in the IVIA5901 and ESVL strains could be an important virulence factor in almond trees, from which they were isolated. It could be speculated that a lower ability to form biofilm may be related to a lower colonization of mouthparts

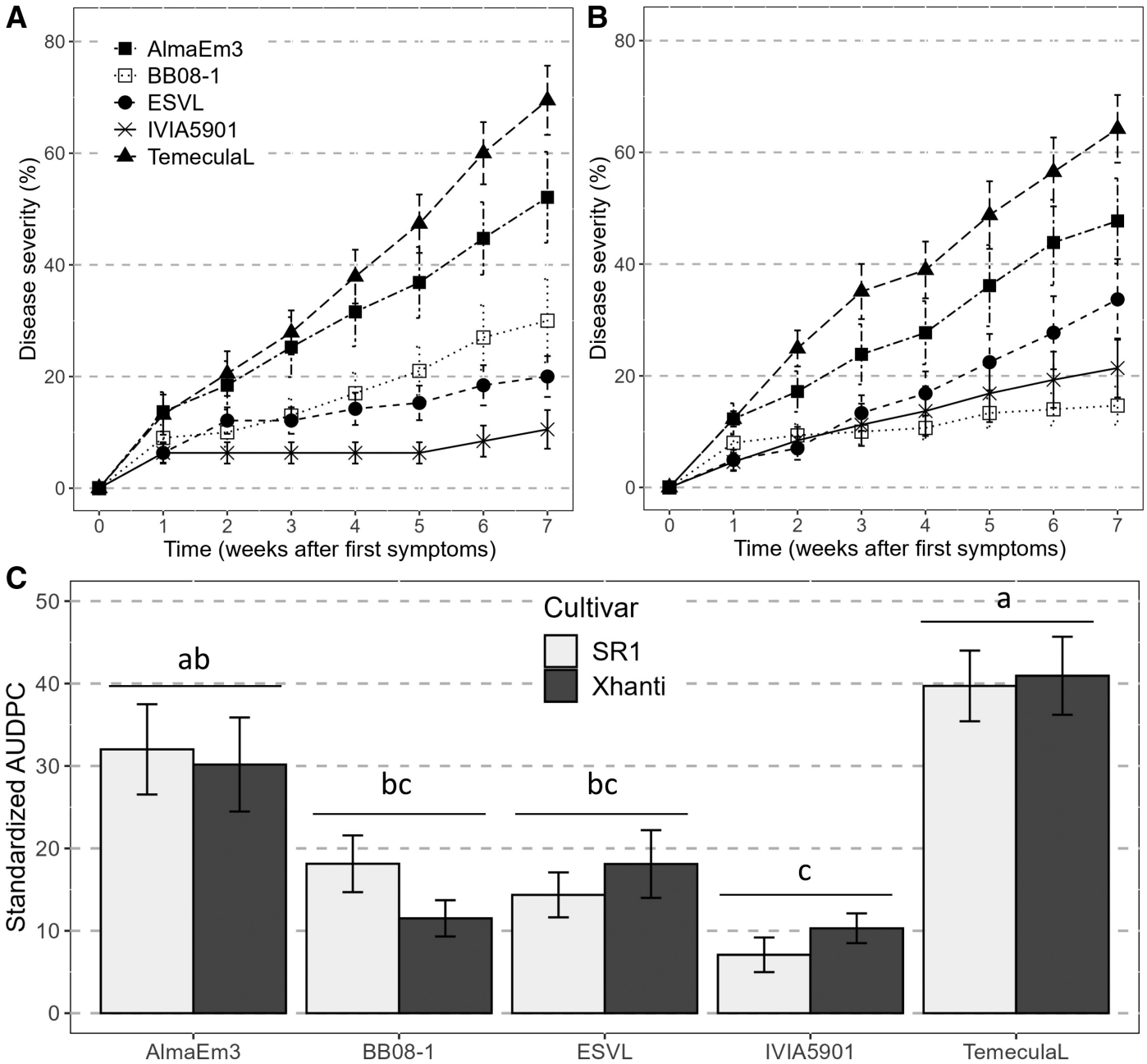

Fig. 6. Disease severity progress curves of symptom development in tobacco plants **A,** 'Petite Havana SR1' and **B,** 'Xanthi.' **C,** Standardized area under the disease severity progress curve (SAUDPC). Plants were inoculated with *Xylella fastidiosa* strains AlmaEm3, BB08-1, ESVL, IVIA5901, and TemeculaL and grown in the greenhouse at 20 to 25°C. Disease severity was estimated by the percentage of leaves showing symptoms per plant. Each point or bar represents the mean value of two independent experiments under the same conditions. Vertical lines represent the standard error of the mean. For SAUDPC values, bar groups for each strain with different letters indicate significant differences ($P < 0.05$) according to a post-hoc protected Tukey's honestly significant difference test.

of the insect vectors, resulting in a lower transmission. However, due to the lack of a latent period in *X. fastidiosa* insect vectors (Purcell 1979), colonization of insect foregut by *X. fastidiosa* is not an essential factor for transmissibility (Chatterjee et al. 2008).

Fimbrial proteins are also involved in the processes of biofilm formation, cell adhesion, and aggregation (De La Fuente et al. 2007b; Feil et al. 2007). Specifically, type IV pili has been described as playing an important role in adhesion to surfaces, early stages of biofilm development, and the formation of macrocolonies (Caserta et al. 2010). Several studies (Cursino et al. 2011; Li et al. 2007; Meng et al. 2005) using mutants defective in type IV pili have shown lower ability to form biofilm, which was also related to a twitching-defective phenotype. Low ability to form biofilm and cell aggregation by Spanish strains may be due not only to the SNPs or truncated proteins found in afimbrial adhesin proteins but also likely to a possible loss of function of type IV pili in both strains. Interestingly, a deleterious amino acid variation in *pilB* and *pilY1* was found in both Spanish strains when compared with the reference strain, Temecula1, which could also explain the phenotype observed. A similar growth behavior to that observed in the Spanish strains when growing in microfluidic chambers was observed in a *pilB* mutant of the Temecula1 strain, which showed smaller aggregates and lace-like structures occupying the entire channel as compared with its wild type (De La Fuente et al. 2008). All these hypotheses will have to be further tested by functional analysis in the Spanish strains.

Interestingly, adhesion force values obtained for the Spanish strains were higher than those described for the Temecula 1 strain, suggesting that the Spanish strains have a higher surface attachment capacity. This high surface attachment capacity has been associated with two *pilB* and *pilY1* mutants of the Temecula1 strain (Cruz et al. 2014; De La Fuente et al. 2007b). It has been suggested that several adhesins are involved in a sequential complex process for biofilm formation and cell-to-cell aggregation (Feil et al. 2007), but also, as demonstrated by Parker et al. (2016), different expression levels for afimbrial and fimbrial genes, which are associated with attach-

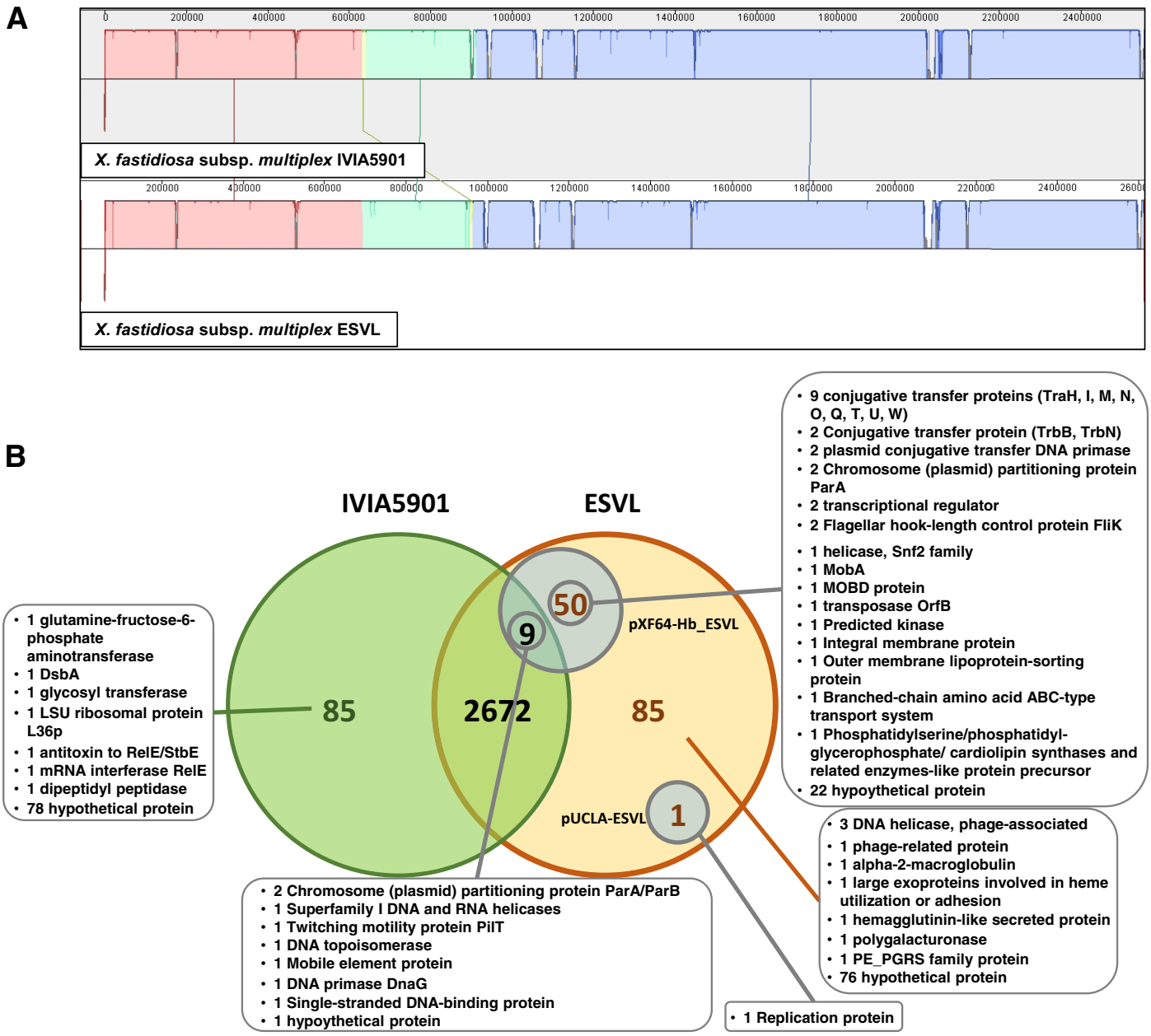

Fig. 7. Comparison of whole genome sequences of *Xylella fastidiosa* strains IVIA5901 and ESVL. **A,** MAUVE progressive alignment. Colored blocks connected by lines indicate syntenic regions. Scale is in base pairs. **B,** Venn diagram showing the number of unique and shared coding sequences between strains.

TABLE 3. Summary of phenotypic traits of the *Xylella fastidiosa* strains used in this study

Trait	Figure/video[a]	Strains[b]				
		Alma-Em3	BB08-1	ESVL	IVIA5901	TemeculaL
Total growth	1A-B	+++	+	+	+++	++
Biofilm formation	1C/2A	+++	+++	+	+	++
Planktonic growth	1D/2A	+	+	++	+++	+++
Settling rate	2B	+++	+++	+	+	+++
Adhesion force (microfluidic chamber)	3B-C (SV1)	np[c]	np	+++	+	+
Twitching speed (microfluidic chamber)	SV 2-3	np	np	++	–	+++
Twitching after 2 days	4B	+	+	++	–	+++
Twitching after 5 days	4B	+	+	–	–	+++
Type I pili (SEM)	5/SF1	np	np	Present	Present	Present
Type IV pili (SEM)	5/SF1	np	np	Present	Present	Present
Cell length (SEM)	5/SF1	np	np	++	+	+++
Tobacco virulence	6	+++	++	++	+	+++

[a] Figure or video in which each trait is shown in this current manuscript. SV, supplementary video; and SF, supplementary figure.
[b] Phenotype level: –, absent; +, low; ++, moderate; and +++, high in relation to the maximum levels reached in each experiment.
[c] np: not performed.

ment, biofilm formation, and motility, occur over time. Thus, the phenotype found in the Spanish strains is probably due to changes in several CDSs and possibly not due to a change in a few single CDSs.

The Spanish IVIA5901 strain did not show twitching motility, although it produces type IV pili. A possible explanation is that these pili are nonfunctional. A similar result was found by Cursino et al. (2011) that showed that a *pilL2* mutant lacking twitching motility presented reduced virulence and biofilm formation compared with the wild-type strain, but it also had a fully developed type IV pili.

By contrast, the ESVL strain was able to move against the flow in the microfluidic chamber and showed twitching motility. This result resembles the observations described for a *pilY1* mutant of the Temecula strain (Li et al. 2007) that had reduced, but not completely absent, twitching motility. We speculate that the potentially deleterious amino acid variation found in the *pilY1* gene of the Spanish strains could be related to their phenotype, as this gene also affects twitching motility but to a lesser extent than other genes that are required for the formation of type IV pili (i.e., *pilO*, *pilR*, *fimT*, and *pilX*) (Li et al. 2007). Interestingly, a reduced or nontwitching ability has been associated with a lower capacity for homologous recombination (Kandel et al. 2017), which is also related to a low ability to form biofilm or aggregate cells, depending on the strain studied. In a recent work testing natural competence in a large collection of *X. fastidiosa* strains, the two Spanish strains included in this study, ESVL and IVIA5901, were not naturally competent (Ranlin et al. 2021). The annotation given by RAST revealed the presence in the plasmid pXF64-Hb_ESVL of strain ESVL of a *pilT* homolog gene related to twitching motility. We speculate that the presence of this extra copy might be fixing the lack of motility found in the IVIA5901 strain because it is the only difference found between these two strains that is annotated as a CDS related to motility.

In addition to the important differences found in traits and CDSs directly related to cell adhesion and motility and the unique CDS found in the plasmid pXF64-Hb_ESVL, our results also showed the presence of some unique CDSs in both the chromosome and the large plasmid that may be relevant for some virulence-related traits. For example, two CDSs found in the chromosome of the IVIA5901 strain (peg.2284 and peg.2285; Supplementary Table S2) have a high similarity to two genes involved in the toxin-antitoxin system *RelE*/*StbE* (PD1183 and PD1184). The function of a similar toxin-antitoxin system (DinJ/RelE) in the control of the bacterial population during plant colonization was previously demonstrated (Burbank and Stenger 2017).

Although previous studies described the presence and genomic characterization of plasmids in some *X. fastidiosa* strains, there is a lack of interpretation of the potential role of those plasmids in processes related to virulence. Our results suggested that the phenotypic differences found between both Spanish strains might be caused by the presence of the two plasmids in the ESVL strain, in addition to the chromosomal differences found. In the Spanish outbreak area of Alicante, where these strains were isolated, three type of strains harboring different plasmid content coexist (i.e., strains with plasmids pXF64-Hb_ESVL and pUCLA-ESVL, strains with plasmid pUCLA-ESVL only, and strains with no plasmids; Velasco-Amo et al. 2019). The differences in virulence in almond, host range, and geographical distribution within the demarcated area of Alicante of these three types of strains deserves further studies to infer the potential role of those plasmids in the adaptation of *X. fastidiosa* to new environments and host plants. Some future studies could include plasmid curation and/or the reconstruction of plasmid sequences in mobilizable plasmids on the basis of their gene sequences to analyze their potential role in virulence.

Acknowledgments

We thank J. C. Rivas for support in TEM analysis and Hongyu Chen, Eber Feliciano, Qing Ge, and Marcus Silva, as members of De La Fuente's laboratory, for their support in the experimental procedures.

Literature Cited

Almeida, R. P. P., De La Fuente, L., Koebnik, R., Lopes, J. R. S., Parnell, S., and Scherm, H. 2019. Addressing the new global threat of *Xylella fastidiosa*. Phytopathology 109:172-174.

Arias-Giraldo, L. F., Giampetruzzi, A., Metsis, M., Marco-Noales, E., Imperial, J., Velasco-Amo, M. P., Román-Écija, M., and Landa, B. B. 2020. Complete circularized genome data of two Spanish strains of *Xylella fastidiosa* (IVIA5235 and IVIA5901) using hybrid assembly approaches. Phytopathology 110:969-972.

Aziz, R. K., Bartels, D., Best, A. A., DeJongh, M., Disz, T., Edwards, R. A., Formsma, K., Gerdes, S., Glass, E. M., Kubal, M., Meyer, F., Olsen, G. J., Olson, R., Osterman, A. L., Overbeek, R. A., McNeil, L. K., Paarmann, D., Paczian, T., Parrello, B., Pusch, G. D., Reich, C., Stevens, R., Vassieva, O., Vonstein, V., Wilke, A., and Zagnitko, O. 2008. The RAST server: Rapid Annotations using Subsystems Technology. BMC Genomics 9:75.

Bogino, P. C., Oliva, M. M., Sorroche, F. G., and Giordano, W. 2013. The role of bacterial biofilms and surface components in plant-bacterial associations. Int. J. Mol. Sci. 14:15838-15859.

Brettin, T., Davis, J. J., Disz, T., Edwards, R. A., Gerdes, S., Olsen, G. J., Overbeek, R., Parrello, B., Pusch, G. D., Shukla, M., Thomason, J. A., III, Stevens, R., Vonstein, V., Wattam, A. R., and Xia, F. 2015. RASTtk: A modular and extensible implementation of the RAST algorithm for building custom annotation pipelines and annotating batches of genomes. Sci. Rep. 5:8365.

Burbank, L. P., and Stenger, D. C. 2017. The DinJ/RelE toxin-antitoxin system suppresses bacterial proliferation and virulence of *Xylella fastidiosa* in grapevine. Phytopathology 107:388-394.

Burbank, L. P., and Van Horn, C. R. 2017. Conjugative plasmid transfer in *Xylella fastidiosa* is dependent on tra and trb operon functions. J. Bacteriol. 199:e00388-17.

Caserta, R., Takita, M. A., Targon, M. L., Rosselli-Murai, L. K., de Souza, A. P., Peroni, L., Stach-Machado, D. R., Andrade, A., Labate, C. A., Kitajima, E. W., Machado, M. A., and de Souza, A. A. 2010. Expression of *Xylella fastidiosa* fimbrial and afimbrial proteins during biofilm formation. Appl. Environ. Microbiol. 76:4250-4259.

Chatterjee, S., Almeida, R. P. P., and Lindow, S. 2008. Living in two worlds: The plant and insect lifestyles of *Xylella fastidiosa*. Annu. Rev. Phytopathol. 46:243-271.

Chen, H., and De La Fuente, L. 2020. Calcium transcriptionally regulates movement, recombination and other functions of *Xylella fastidiosa* under constant flow inside microfluidic chambers. Microb. Biotechnol. 13: 548-561.

Chen, H., Kandel, P. P., Cruz, L. F., Cobine, P. A., and De La Fuente, L. 2017. The major outer membrane protein MopB is required for twitching movement and affects biofilm formation and virulence in two *Xylella fastidiosa* strains. Mol. Plant-Microbe Interact. 30:896-905.

Chen, J., Civerolo, E. L., Jarret, R. L., Sluys, M.-A. V., and Oliveira, M. C. 2005. Genetic discovery in *Xylella fastidiosa* through sequence analysis of selected randomly amplified polymorphic DNAs. Curr. Microbiol. 50:78-83.

Choi, Y., and Chan, A. P. 2015. PROVEAN web server: A tool to predict the functional effect of amino acid substitutions and indels. Bioinformatics 31:2745-2747.

Colnaghi Simionato, A. V., da Silva, D. S., Lambais, M. R., and Carrilho, E. 2007. Characterization of a putative *Xylella fastidiosa* diffusible signal factor by HRGC-EI-MS. J. Mass Spectrom. 42:1375-1381.

Cruz, L. F., Cobine, P. A., and De La Fuente, L. 2012. Calcium increases *Xylella fastidiosa* surface attachment, biofilm formation, and twitching motility. Appl. Environ. Microbiol. 78:1321-1331.

Cruz, L. F., Parker, J. K., Cobine, P. A., and De La Fuente, L. 2014. Calcium-enhanced twitching motility in *Xylella fastidiosa* is linked to a single PilY1 homolog. Appl. Environ. Microbiol. 80:7176-7185.

Cursino, L., Galvani, C. D., Athinuwat, D., Zaini, P. A., Li, Y., De La Fuente, L., Hoch, H. C., Burr, T. J., and Mowery, P. 2011. Identification of an operon, Pil-Chp, that controls twitching motility and virulence in *Xylella fastidiosa*. Mol. Plant-Microbe Interact. 24:1198-1206.

Darling, A. C. E., Mau, B., Blattner, F. R., and Perna, N. T. 2004. Mauve: Multiple alignment of conserved genomic sequence with rearrangements. Genome Res. 14:1394-1403.

D'Attoma, G., Morelli, M., De La Fuente, L., Cobine, P. A., Saponari, M., de Souza, A. A., De Stradis, A., and Saldarelli, P. 2020. Phenotypic characterization and transformation attempts reveal peculiar traits of *Xylella fastidiosa* subspecies *pauca* strain De Donno. Microorganisms 8:1832.

Davis, M. J. 1980. Isolation media for the Pierce's disease bacterium. Phytopathology 70:425.

Davis, M. J., French, W. J., and Schaad, N. W. 1981. Axenic culture of the bacteria associated with phony disease of peach and plum leaf scald. Curr. Microbiol. 6:309-314.

De La Fuente, L., Burr, T. J., and Hoch, H. C. 2007a. Mutations in type I and type IV pilus biosynthetic genes affect twitching motility rates in *Xylella fastidiosa*. J. Bacteriol. 189:7507-7510.

De La Fuente, L., Montanes, E., Meng, Y., Li, Y., Burr, T. J., Hoch, H. C., and Wu, M. 2007b. Assessing adhesion forces of type I and type IV pili of *Xylella fastidiosa* bacteria by use of a microfluidic flow chamber. Appl. Environ. Microbiol. 73:2690-2696.

De La Fuente, L., Burr, T. J., and Hoch, H. C. 2008. Autoaggregation of *Xylella fastidiosa* cells is influenced by type I and type IV pili. Appl. Environ. Microbiol 74:5579-5582.

De La Fuente, L., Parker, J. K., Oliver, J. E., Granger, S., Brannen, P. M., van Santen, E., and Cobine, P. A. 2013. The bacterial pathogen *Xylella fastidiosa* affects the leaf ionome of plant hosts during infection. PLoS One 8: e62945.

de Mendiburu, F. 2020. agricolae: Statistical Procedures for Agricultural Research. https://CRAN.R-project.org/package=agricolae (accessed May 9, 2020).

de Souza, J. B., Almeida-Souza, H. O., Zaini, P. A., Alves, M. N., de Souza, A. G., Pierry, P. M., da Silva, A. M., Goulart, L. R., Dandekar, A. M., and Nascimento, R. 2020. *Xylella fastidiosa* subsp. *pauca* strains Fb7 and 9a5c from citrus display differential behavior, secretome, and plant virulence. Int. J. Mol. Sci. 21:6769.

Delbianco, A., Gibin, D., Pasinato, L., and Morelli, M. 2022. Update of the *Xylella* spp. host plant database – systematic literature search up to 30 June 2021. EFSA J. 20:e07039.

Denancé, N., Briand, M., Gaborieau, R., Gaillard, S., and Jacques, M. A. 2019. Identification of genetic relationships and subspecies signatures in *Xylella fastidiosa*. BMC Genomics 20:1-21.

DOGV. 2021. Diario oficial de la Generalidad Valenciana. Resolución de 29 de noviembre de 2021, del director general de Agricultura, Ganadería y Pesca, por la cual se declara la decimosexta actualización de la situación de la plaga *Xylella fastidiosa* (Wells et al.) en el territorio de la Comunitat Valenciana y se adoptan medidas fitosanitarias urgentes de erradicación y control para evitar su propagación.

EFSA Panel on Plant Health (PLH), Bragard, C., Dehnen-Schmutz, K., Di Serio, F., Gonthier, P., Jacques, M.-A., Jaques Miret, J. A., Justesen, A. F., MacLeod, A., Magnusson, C. S., Milonas, P., Navas-Cortés, J. A., Potting, R., Reignault, P. L., Thulke, H.-H., van der Werf, W., Vicent Civera, A., Yuen, J., Zappalà, L., Boscia, D., Chapman, D., Gilioli, G., Krugner, R., Mastin, A., Simonetto, A., Spotti Lopes, J. R., White, S., Abrahantes, J. C., Delbianco, A., Maiorano, A., Mosbach-Schulz, O., Stancanelli, G., Guzzo, M., and Parnell, S. 2019. Update of the scientific opinion on the risks to plant health posed by *Xylella fastidiosa* in the EU territory. EFSA J. 17:e05665.

Feil, H., Feil, W. S., and Lindow, S. E. 2007. Contribution of fimbrial and afimbrial adhesins of *Xylella fastidiosa* to attachment to surfaces and virulence to grape. Phytopathology 97:318-324.

Galvani, C. D., Li, Y., Burr, T. J., and Hoch, H. C. 2007. Twitching motility among pathogenic *Xylella fastidiosa* isolates and the influence of bovine serum albumin on twitching-dependent colony fringe morphology. FEMS Microbiol. Lett. 268:202-208.

Giampetruzzi, A., Morelli, M., Saponari, M., Loconsole, G., Chiumenti, M., Boscia, D., Savino, V. N., Martelli, G. P., and Saldarelli, P. 2016. Transcriptome profiling of two olive cultivars in response to infection by the CoDiRO strain of *Xylella fastidiosa* subsp. *pauca*. BMC Genomics 17:475.

Giampetruzzi, A., Velasco-Amo, M. P., Marco-Noales, E., Montes-Borrego, M., Román-Écija, M., Navarro, I., Monterde, A., Barbé, S., Almeida, R. P. P., Saldarelli, P., Saponari, M., Montilon, V., Boscia, D., and Landa, B. B. 2019. Draft genome resources of two strains ("ESVL" and "IVIA5901") of *Xylella fastidiosa* associated with almond leaf scorch disease in Alicante. Spain. Phytopathology 109:219-221.

Gouran, H., Gillespie, H., Nascimento, R., Chakraborty, S., Zaini, P. A., Jacobson, A., Phinney, B. S., Dolan, D., Durbin-Johnson, B. P., Antonova, E. S., Lindow, S. E., Mellema, M. S., Goulart, L. R., and Dandekar, A. M. 2016. The secreted protease PrtA controls cell growth, biofilm formation and pathogenicity in *Xylella fastidiosa*. Sci. Rep. 6:31098.

Guilhabert, M. R., and Kirkpatrick, B. C. 2005. Identification of *Xylella fastidiosa* antivirulence genes: Hemagglutinin adhesins contribute to *X. fastidiosa* biofilm maturation and colonization and attenuate virulence. Mol. Plant-Microbe Interact. 18:856-868.

Guilhabert, M. R., Stewart, V. J., and Kirkpatrick, B. C. 2006. Characterization of putative rolling-circle plasmids from the Gram-negative bacterium *Xylella fastidiosa* and their use as shuttle vectors. Plasmid 55:70-80.

Hao, L., Johnson, K., Cursino, L., Mowery, P., and Burr, T. J. 2017. Characterization of the *Xylella fastidiosa* PD1311 gene mutant and its suppression of Pierce's disease on grapevines. Mol. Plant Pathol. 18:684-694.

Hendson, M., Purcell, A. H., Chen, D., Smart, C., Guilhabert, M., and Kirkpatrick, B. 2001. Genetic diversity of Pierce's disease strains and other pathotypes of *Xylella fastidiosa*. Appl. Environ. Microbiol. 67:895-903.

Hopkins, D. L. 1989. *Xylella fastidiosa*: Xylem-limited bacterial pathogen of plants. Annu. Rev. Phytopathol. 27:271-290.

Hunt, M., Silva, N. D., Otto, T. D., Parkhill, J., Keane, J. A., and Harris, S. R. 2015. Circlator: Automated circularization of genome assemblies using long sequencing reads. Genome Biol. 16:294.

Kandel, P. P., Almeida, R. P. P., Cobine, P. A., and De La Fuente, L. 2017. Natural competence rates are variable among *Xylella fastidiosa* strains and homologous recombination occurs *in vitro* between subspecies *fastidiosa* and *multiplex*. Mol. Plant-Microbe Interact. 30:589-600.

Kandel, P. P., Chen, H., and De La Fuente, L. 2018. A short protocol for gene knockout and complementation in *Xylella fastidiosa* shows that one of the type IV pilin paralogs (PD1926) is needed for twitching while another (PD1924) affects pilus number and location. Appl. Environ. Microbiol. 84: e01167-18.

Killiny, N., and Almeida, R. P. P. 2009. *Xylella fastidiosa* afimbrial adhesins mediate cell transmission to plants by leafhopper vectors. Appl. Environ. Microbiol. 75:521-528.

Koide, T., Zaino, P. A., Moreira, L. M., Vencio, R. Z., Matsukuma, A. Y., Durham, A. M., Teixeira, D. C., El-Dorry, H., Monteiro, P. B., da Silva, A. C., Verjovski-Almeida, S., da Silva, A. M., and Gomes, S. L. 2004. DNA microarray-based genome comparison of a pathogenic and a nonpathogenic strain of *Xylella fastidiosa* delineates genes important for bacterial virulence. J. Bacteriol. 186:5442-5449.

Kolmogorov, M., Yuan, J., Lin, Y., and Pevzner, P. A. 2019. Assembly of long, error-prone reads using repeat graphs. Nat. Biotechnol. 37:540-546.

Li, Y., Hao, G., Galvani, C. D., Meng, Y., De La Fuente, L., Hoch, H. C., and Burr, T. J. 2007. Type I and type IV pili of *Xylella fastidiosa* affect twitching motility, biofilm formation and cell-cell aggregation. Microbiology 153:719-726.

Madeira, F., Park, Y. M., Lee, J., Buso, N., Gur, T., Madhusoodanan, N., Basutkar, P., Tivey, A. R. N., Potter, S. C., Finn, R. D., and Lopez, R. 2019. The EMBL-EBI search and sequence analysis tools APIs in 2019. Nucleic Acids Res. 47:W636-W641.

Marcelletti, S., and Scortichini, M. 2016. Genome-wide comparison and taxonomic relatedness of multiple *Xylella fastidiosa* strains reveal the occurrence of three subspecies and a new *Xylella* species. Arch. Microbiol. 198: 803-812.

Marco-Noales, E., Barbé, S., Monterde, A., Navarro-Herrero, I., Ferrer, A., Dalmau, V., Aure, C. M., Domingo-Calap, M. L., Landa, B. B., and Roselló, M. 2021. Evidence that *Xylella fastidiosa* is the causal agent of almond leaf scorch disease in Alicante, mainland Spain (Iberian Peninsula). Plant Dis. 105:3349-3352.

Meng, Y., Li, Y., Galvani, C. D., Hao, G., Turner, J. N., Burr, T. J., and Hoch, H. C. 2005. Upstream migration of *Xylella fastidiosa* via pilus-driven twitching motility. J. Bacteriol. 187:5560-5567.

Monteiro-Vitorello, C. B., De Oliveira, M. C., Zerillo, M. M., Varani, A. M., Civerolo, E., and Sluys, M. A. V. 2005. *Xylella* and *Xanthomonas* Mobil'omics. OMICS J. Integr. Biol. 9:146-159.

Moralejo, E., Gomila, M., Montesinos, M., Borràs, D., Pascual, A., Nieto, A., Adrover, F., Gost, P. A., Seguí, G., Busquets, A., Jurado-Rivera, J. A., Quetglas, B., García, J. D., Beidas, O., Juan, A., Velasco-Amo, M. P., Landa, B. B., and Olmo, D. 2020. Phylogenetic inference enables reconstruction of a long-overlooked outbreak of almond leaf scorch disease (*Xylella fastidiosa*) in Europe. Commun. Biol. 3:1-13.

Newman, K. L., Almeida, R. P. P., Purcell, A. H., and Lindow, S. E. 2004. Cell-cell signaling controls *Xylella fastidiosa* interactions with both insects and plants. Proc. Natl. Acad. Sci. 101:1737-1742.

Nunney, L., Azad, H., and Stouthamer, R. 2019. An experimental test of the host-plant range of nonrecombinant strains of North American *Xylella fastidiosa* subsp. *multiplex*. Phytopathology 109:294-300.

O'Leary, M. L., Arias-Giraldo, L. F., Burbank, L. P., De La Fuente, L., and Landa, B. B. 2022. Complete genome resources for *Xylella fastidiosa* strains AlmaEM3 and BB08-1 reveal prophage-associated structural variation among blueberry-infecting strains. Phytopathology 112:732-736.

Oliver, J. E., Sefick, S. A., Parker, J. K., Arnold, T., Cobine, P. A., and De La Fuente, L. 2014. Ionome changes in *Xylella fastidiosa*-infected *Nicotiana tabacum* correlate with virulence and discriminate between subspecies of bacterial isolates. Mol. Plant-Microbe Interact. 27:1048-1058.

Overbeek, R., Olson, R., Pusch, G. D., Olsen, G. J., Davis, J. J., Disz, T., Edwards, R. A., Gerdes, S., Parrello, B., Shukla, M., Vonstein, V., Wattam, A. R., Xia, F., and Stevens, R. 2014. The SEED and the Rapid Annotation of microbial genomes using Subsystems Technology (RAST). Nucleic Acids Res. 42:D206-D214.

Parker, J. K., Chen, H., McCarty, S. E., Liu, L. Y., and De La Fuente, L. 2016. Calcium transcriptionally regulates the biofilm machinery of *Xylella fastidiosa* to promote continued biofilm development in batch cultures. Environ. Microbiol. 18:1620-1634.

Pierry, P. M., Uceda-Campos, G., Feitosa-Junior, O. R., Martins-Junior, J., de Santana, W. O., Coletta-Filho, H. D., Zaini, P. A., and da-Silva, A. M. 2020. Genetic diversity of *Xylella fastidiosa* plasmids assessed by comparative genomics. Trop. Plant Pathol. 45:342-360.

Pooler, M. R., Hartung, J. S., and Fenton, R. G. 1997. Sequence analysis of a 1296-nucleotide plasmid from *Xylella fastidiosa*. FEMS Microbiol. Lett. 155:217-222.

Potnis, N., Kandel, P. P., Merfa, M. V., Retchless, A. C., Parker, J. K., Stenger, D. C., Almeida, R. P. P., Bergsma-Vlami, M., Westenberg, M., Cobine, P. A., and De La Fuente, L. 2019. Patterns of inter- and intrasubspecific homologous recombination inform eco-evolutionary dynamics of *Xylella fastidiosa*. ISME J. 13:2319-2333.

Purcell, A. H. 1979. Evidence for noncirculative transmission of Pierce's disease bacterium by sharpshooter leafhoppers. Phytopathology 69:393.

R Core Team. 2020. R: A language and environment for statistical computing. R Foundation for Statistical Computing, Vienna, Austria. https://www.R-project.org/

Ranlin, L., Castillo Siri, A., Arias-Giraldo, L. F., Velasco Amo, M. P., Almeida, R. P., Landa, B. B., Potnis, N., and De La Fuente, L. 2021. Natural competence and homologous recombination among *Xylella fastidiosa* strains. 3rd European Conference on *Xylella fastidiosa* and XF-ACTORS final meeting. https://zenodo.org/record/4678393#.YJYyTaHtbIX

Rogers, E. E., and Stenger, D. C. 2012. A conjugative 38 kB plasmid is present in multiple subspecies of *Xylella fastidiosa*. PLoS One 7:e52131.

Roper, C., Castro, C., and Ingel, B. 2019. *Xylella fastidiosa*: Bacterial parasitism with hallmarks of commensalism. Curr. Opin. Plant Biol. 50: 140-147.

Rueden, C. T., Schindelin, J., Hiner, M. C., DeZonia, B. E., Walter, A. E., Arena, E. T., and Eliceiri, K. W. 2017. ImageJ2: ImageJ for the next generation of scientific image data. BMC Bioinf. 18:1-26.

Sakia, R. M. 1992. The Box-Cox transformation technique: A review. J. R. Stat. Soc. Ser. Stat. 41:169-178.

Saponari, M., Boscia, D., Altamura, G., Loconsole, G., Zicca, S., D'Attoma, G., Morelli, M., Palmisano, F., Saponari, A., Tavano, D., Savino, V. N., Dongiovanni, C., and Martelli, G. P. 2017. Isolation and pathogenicity of *Xylella fastidiosa* associated to the olive quick decline syndrome in southern Italy. Sci. Rep. 7:17723.

Saponari, M., D'Attoma, G., Abou Kubaa, R., Loconsole, G., Altamura, G., Zicca, S., Rizzo, D., and Boscia, D. 2019. A new variant of *Xylella fastidiosa* subspecies *multiplex* detected in different host plants in the recently emerged outbreak in the region of Tuscany, Italy. Eur. J. Plant Pathol. 154:1195-1200.

Saponari, M., Giampetruzzi, A., Loconsole, G., Boscia, D., and Saldarelli, P. 2018. *Xylella fastidiosa* in olive in Apulia: Where we stand. Phytopathology 109:175-186.

Sengupta, M., and Austin, S. 2011. Prevalence and significance of plasmid maintenance functions in the virulence plasmids of pathogenic bacteria. Infect. Immun. 79:2502-2509.

Shi, X. Y., Dumenyo, C. K., Hernandez-Martinez, R., Azad, H., and Cooksey, D. A. 2007. Characterization of regulatory pathways in *Xylella fastidiosa*: Genes and phenotypes controlled by *algU*. Appl. Environ. Microbiol. 73:6748-6756.

Sicard, A., Zeilinger, A. R., Vanhove, M., Schartel, T. E., Beal, D. J., Daugherty, M. P., and Almeida, R. P. P. 2018. *Xylella fastidiosa*: Insights into an emerging plant pathogen. Annu. Rev. Phytopathol. 56:181-202.

Simko, I., and Piepho, H. P. 2011. The area under the disease progress stairs: Calculation, advantage, and application. Phytopathology 102:381-389.

Simpson, A. J., Reinach, F. C., Arruda, P., Abreu, F. A., Acencio, M., Alvarenga, R., Alves, L. M., Araya, J. E., Baia, G. S., Baptista, C. S., Barros, M. H., Bonaccorsi, E. D., Bordin, S., Bove, J. M., Briones, M. R., Bueno, M. R., Camargo, A. A., Camargo, L. E., Carraro, D. M., Carrer, H., Colauto, N. B., Colombo, C., Costa, F. F., Costa, M. C., Costa-Neto, C. M., Coutinho, L. L., Cristofani, M., Dias-Neto, E., Docena, C., El-Dorry, H., Facincani, A. P., Ferreira, A. J., Ferreira, V. C., Ferro, J. A., Fraga, J. S., Franca S. C., Franco, M. C., Frohme, M., Furlan, L. R., Garnier, M., Goldman, G. H., Goldman, M. H., Gomes, S. L., Gruber, A., Ho, P. L., Hoheisel, J. D., Junqueira, M. L., Kemper, E. L., Kitajima, J. P., Krieger, J. E., Kuramae, E. E., Laigret, F., Lambais, M. R., Leite, L. C., Lemos, E. G., Lemos, M. V., Lopes, S. A., Lopes, C. R., Machado, J. A., Machado, M. A., Madeira, A. M., Madeira, H. M., Marino, C. L., Marques, M. V., Martins, E. A., Martins, E. M., Matsukuma, A. Y., Menck, C. F., Miracca, E. C., Miyaki, C. Y., Monteriro-Vitorello, C. B., Moon, D. H., Nagai, M. A., Nascimento, A. L., Netto, L. E., Nhani, A., Jr., Nobrega, F. G., Nunes, L. R., Oliveira, M. A., de Oliveira, M. C., de Oliveira, R. C., Palmieri, D. A., Paris, A., Peixoto, B. R., Pereira, G. A., Pereira, H. A., Jr., Pesquero, J. B., Quaggio, R. B., Roberto, P. G., Rodrigues, V., de M Rosa, A. J., de Rosa, V. E., Jr., de Sa, R. G., Santelli, R. V., Sawasaki, H. E., da Silva, A. C., da Silva, A. M., da Silva, F. R., da Silva, W. A., Jr., da Silveira, J. F., Silvestri, M. L., Siqueira, W. J., de Souza, A. A., de Souza, A. P., Terenzi, M. F., Truffi, D., Tsai, S. M., Tsuhako, M. H., Vallada, H., Van Sluys, M. A., Verjovski-Almeida, S., Vettore, A. L., Zago, M. A., Zatz, M., Meidanis, J., and Setubal, J. C. 2000. The genome sequence of the plant pathogen *Xylella fastidiosa*: The *Xylella fastidiosa* consortium of the organization for nucleotide sequencing and analysis, Sao Paulo, Brazil. Nature 406:151-157.

Sørensen, S. J., Bailey, M., Hansen, L. H., Kroer, N., and Wuertz, S. 2005. Studying plasmid horizontal transfer *in situ*: A critical review. Nat. Rev. Microbiol. 3:700-710.

Stenger, D. C., Lee, M. W., Rogers, E. E., and Chen, J. 2010. Plasmids of *Xylella fastidiosa* mulberry-infecting strains share extensive sequence identity and gene complement with pVEIS01 from the earthworm symbiont *Verminephrobacter eiseniae*. Physiol. Mol. Plant Pathol. 74: 238-245.

Vanhove, M., Retchless, A. C., Sicard, A., Rieux, A., Coletta-Filho, H. D., De La Fuente, L., Stenger, D. C., and Almeida, R. P. P. 2019. Genomic diversity and recombination among *Xylella fastidiosa* subspecies. Appl. Environ. Microbiol. 85:e02972-18.

Velasco-Amo, M. P., Román-Écija, M., Montes Borrego, M., Olivares-García, C., Giampetruzzi, A., Navas Cortés, J. A., and Landa, B. B. 2019. Occurrence of plasmids pXF64-Hb_ESVL and pUCLA-ESVL associated with infections caused by *Xylella fastidiosa* subsp. *multiplex* ST6 in the demarcated area of Alicante. Spain. 2nd Eur. Conf. *Xylella fastidiosa* 2019 EFSA. https://digital.csic.es/handle/10261/207917 (accessed May 12, 2020).

Venables, W. N., and Ripley, B. D. 2013. Modern Applied Statistics with S-PLUS. Springer Science & Business Media, New York.

Vivian, A., Murillo, J., and Jackson, R. W. 2001. The roles of plasmids in phytopathogenic bacteria: Mobile arsenals? Microbiol. Read. Engl. 147: 763-780.

Wang, N., Li, J. L., and Lindow, S. E. 2012. RpfF-dependent regulon of *Xylella fastidiosa*. Phytopathology 102:1045-1053.

Wang, P., Lee, Y., Igo, M. M., and Roper, M. C. 2017. Tolerance to oxidative stress is required for maximal xylem colonization by the xylem-limited bacterial phytopathogen, *Xylella fastidiosa*. Mol. Plant Pathol. 18:990-1000.

Wei, W., Sawyer, T., and Burbank, L. 2021. Csp1, a cold shock protein homolog in *Xylella fastidiosa* influences cell attachment, pili formation, and gene expression. Microbiol. Spectr. 9:e01591-21.

Zaini, P. A., De La Fuente, L., Hoch, H. C., and Burr, T. J. 2009. Grapevine xylem sap enhances biofilm development by *Xylella fastidiosa*. FEMS Microbiol. Lett. 295:129-134.

Zhang, S., Chakrabarty, P. K., Fleites, L. A., Rayside, P. A., Hopkins, D. L., and Gabriel, D. W. 2015. Three new pierce's disease pathogenicity effectors identified using *Xylella fastidiosa* biocontrol strain EB92-1. PLoS One 10:e0133796.

Zimin, A. V., and Salzberg, S. L. 2020. The genome polishing tool POLCA makes fast and accurate corrections in genome assemblies. PLoS Comput. Biol. 16:e1007981.